63 3-5

ASD-TDR-63-131

Investigation of Flow Variables Over a Series of Rearward Facing Stepped Flat Plates at a Nominal Mach Number of 4.15

Richard R. Smith

TECHNICAL DOCUMENTARY REPORT NO. ASD-TDR-63-131

April 1963

Aerodynamics Division
Directorate of Engineering Test
Deputy for Test and Support
Air Force Systems Command
Wright-Patterson Air Force Base, Ohio

Project No. 1366, Task No. 136607

NOTICES

When Government drawings, specifications, or other data are used for any purpose other than in connection with a definitely related Government procurement operation, the United States Government thereby incurs no responsibility nor any obligation whatsoever; and the fact that the Government may have formulated, furnished, or in any way supplied the said drawings, specifications, or other data, is not to be regarded by implication or otherwise as in any manner licensing the holder or any other person or corporation, or conveying any rights or permission to manufacture, use, or sell any patented invention that may in any way be related thereto.

Qualified requesters may obtain copies of this report from the Armed Services Technical Information Agency, (ASTIA), Arlington Hall Station, Arlington 12, Virginia.

This report has been released to the Office of Technical Services, U.S. Department of Commerce, Washington 25, D.C., in stock quantities for sale to the general public.

Copies of this report should not be returned to the Aeronautical Systems Division unless return is required by security considerations, contractual obligations, or notice on a specific document.

28-703T, 400, 5-21-63

FOREWORD

This report was prepared by the High Temperature Section of the Aerodynamics Division, Aeronautical Systems Division, Wright-Patterson Air Force Base, Ohio. The work was accomplished under Task No. 136607, "Hypersonic Gasdynamic Heating," of Project No. 1366, "Aerodynamics and Flight Mechanics" at the request of Richard D. Neumann of the Flight Dynamics Laboratory of ASD.

ABSTRACT

A study was made of the aerodynamic characteristics over a flat plate with basic changes in the flow field imposed by geometric and aerodynamic means. Pressure distributions and schlieren photographs were used to show the effects of (1) leading edge bluntness, (2) rearward facing step, (3) rearward facing step with gas ejected from the vertical face of the step, and (4) a control surface. Although three dimensional effects were large at high angles of attack, the flat plate results correlated well with theory and other experimental data. The effects of leading edge bluntness, step height, and ejection angle are small. The effect of gas ejection, in the manner tested, is not sufficient to produce the effect of a physical control surface.

This technical documentary report has been reviewed and is approved.

Robert L. Colligan Jr.

ROBERT L. COLLIGAN, JR.
Colonel, USAF
Deputy for Test and Support

APPROVAL AND COORDINATION OF ASD-TDR-63-131

PREPARED BY:

Richard R. Smith
RICHARD R. SMITH
Aerospace Project Engineer
Aerodynamics Division

CONCURRED IN:

Carl C. Reichert
for WILLIAM J. DuBOIS
LT COLONEL, USAF
Director Engineering Test
Deputy for Test and Support

CONCURRED IN:

Hugh S. Lippman
HUGH S. LIPPMAN
Technical Director
Deputy for Test and Support

APPROVED BY:

Robert L. Colligan Jr
ROBERT L. COLLIGAN, JR
COLONEL, USAF
Deputy for Test and Support

TABLE OF CONTENTS

ILLUSTRATIONS

ILLUSTRATIONS (CONT'D)

ILLUSTRATIONS (CONT'D)

SYMBOLS

α	angle of attack, degrees
d	Leading Edge (L E) diameter, inches
c	constant in linear viscosity-temperature law
γ	ratio of specific heats of air
M	Mach number
P_∞	free stream static pressure, psia
P_j	static pressure at exit of helium ejection slot, psia
P_m	model surface pressure, psia
P_o	tunnel stagnation pressure, psia
P_{m_5}	model surface pressure at tap #5, psia
Re	Reynolds number per unit length
t	L E thickness, inches
T_o	tunnel stagnation temperature, °R
x	distance from L E , inches
$\bar{X}$	hypersonic interaction parameter, $\frac{M_\infty^3 \sqrt{c}}{\sqrt{Re}}$
X	$f(\bar{X})$

SUBSCRIPTS

i	inviscid
v	viscous
∞	free stream conditions
j	exit conditions of helium ejection slot

ABBREVIATIONS

L E	leading edge
HTF	High Temperature Facility

INTRODUCTION

The purpose of this study was to obtain experimental information on the aerodynamic characteristics over a flat plate with basic changes in the flow field imposed by geometric and aerodynamic means. Pressure distributions and schlieren photographs were used to determine the effects. The effects of (1) leading edge bluntness, (2) rearward facing step, (3) rearward facing step with gas ejected from the vertical face of the step, and (4) a control surface were compared with the basic flat plate data. The data were also compared with existing theories and other experimental work.

The tests were performed in the High Temperature Hypersonic Gasdynamics Facility of the Aeronautical Systems Division. Test efforts were initiated on 15 March 1962 and were completed 22 March 1962. Model pressure distributions were obtained for various free stream test conditions.

TEST EQUIPMENT

All tests were run in the ASD High Temperature, Hypersonic Gasdynamics Facility (HTF) which is described in reference 1. Figure 1 is a schematic diagram of the tunnel and its related systems. The tunnel has a Mach 4 conical nozzle of 5-in. exit diameter and a 10½-in. long open jet test section. Calibration of the test section was done using two asymmetric total head rakes and a water-cooled total head probe as described in reference 2.

Operating ranges for the tests were 300 to 600 psia total pressure and 2500° to 4500°R total temperature, while operating times were on the order of 5 to 10 minutes.

Both "still" and "movie" schlieren coverage was made of all test conditions through the windows of the plenum chamber.

The models were supported by means of the rotating hub, figure 2, which for this test, held three models which could be rotated in and out of the hypersonic stream as desired. Pressure orifice-to-capsule connections were made from model to model by means of a pressure switch which connected the capsules to the model entering the stream.

The gas ejection system, employing a Grove pilot operated regulator, is shown schematically in figure 3. From the gas ejection control panel it was possible to monitor the helium supply pressure, the control pressure to the Grove regulator, and the operation of the open-close solenoid. This system was operable either manually or automatically in conjunction with the rotating hub.

The pressure capsules were referenced to atmosphere and were enclosed in a temperature controlled container, which was located outside the facility plenum chamber.

Manuscript released by the author January 1963 for publication as an ASD Technical Documentary Report.

MODELS AND TEST PROCEDURE

The test models were of two basic shapes: a flat plate with a rearward facing step, and a flat plate with a control surface ramp on the aft end.

Model Nos. 1 through 8 were step models of varying step height and gas ejection angle. Figure 4 is a rear quarter view of Model No. 1 with 0.1-in. nose radius and 0.375-in. step height showing the gas ejection slot. The location of the orifices and the helium ejection slot is shown in figure 5. The models in this series were 2 in. wide and 5 in. long with the step being 3 in. from the Leading Edge.

Model No. 9 was a full flat plate model and served as the reference for the test.

Model Nos. 10 through 13 were the ramp models, with ramps of 5, 10, 20, and 30 degrees, respectively. Figure 6 shows the 5-degree ramp model. The position of the pressure orifices on the ramp models is shown in figure 7. These models were 2 in. wide and 5 in. long with the ramp beginning 3 in. from the L E.

Table 1 lists the various models and the physical characteristics of each.

The gas ejection models, Nos. 1 through 7, had a plenum chamber inside the model which was instrumented to determine pressure and temperature of the gas before ejection. The ejection slot measured .0312 in. wide by 1.25 in. long.

The two gas ejection models and one ramp model were mounted on the rotating hub for each run. Surface pressures were measured at 0, 5, 9.5, and 13.5-degree angles of attack. In addition, models 8, 9, and 10 were tested at both 300 and 600 psi total pressure.

Maximum Reynolds number variation was obtained by testing at minimum pressure-maximum temperature and maximum pressure-minimum temperature. Three different gas ejection pressures were used to determine the effect of this parameter.

RESULTS AND DISCUSSIONS

General

The thirteen models described in table 1 were tested over the range of parameters listed in table 3. The final reduced data for all test conditions has previously been made available to the initiator and are also available from the test project engineer. This report includes sufficient pressure distributions in graphical form to show how the flow field was affected by the various test conditions.

Reference Pressure

Since the HTF conical nozzle was used for this study, there existed a pressure gradient along the nozzle axis due to the diverging flow. Therefore, it was necessary to establish some method of normalizing the surface pressures. The method used consisted of plotting the flat plate pressure distribution (Model No. 9) and fairing it until the distribution indicated it had reached free stream pressure. This pressure was chosen as the numerical value of the free stream pressure for the measured P_0 and T_0 at that instant. Now the measured P_0 and the extrapolated P_∞ were substituted into the isentropic flow equation

for $M = M(P_\infty/P_0)$ and corrected for real gas effects. This gave a Mach number related to the T_0 at the instant under consideration. Then using figure 6 of ASTEA ETR 62-4R, "Calibration of the HTF 5-Inch Conical Nozzle" (ref 2), it was possible to arrive at a relationship between Mach No. and T_0 for all the test runs. Thus P_∞ was indirectly established as a function of the measured T_0. This method allowed a rapid means of normalizing the surface pressures and did not require an extensive change in the data reduction programs. The results have been compared with experimental results of Creager (ref 5) in figure 35; the agreement is considered good.

Surface Pressures

The surface pressures were measured over the angle of attack range of 0 to -13.5 degrees with 3 gas ejection pressures at each angle of attack.

The effect on the pressure distribution of step height, gas ejection angle, and leading edge bluntness will be shown.

One of the principle areas of interest in this test lay in the feasibility of using an ejecting gas to produce control forces similar to those produced by a physical control surface. It may be seen from figures 10 through 16, gas ejection parallel to the step and at an angle of 10 degrees up and 10 degrees down, produces a sharp pressure rise immediately behind the step. As the ejection gas fully expands this pressure rise falls off almost as sharply as it rose. This rise and fall of pressure is of too short a duration to produce a distribution similar to those of the control surface models of figures 19 through 22. The schlieren photographs of figure 8 show the shock wave produced by ejecting helium over model No. 3. These are typical of all the step models. While this wave is fairly strong it is much weaker than the shock wave from the control surface models, figure 9. This indicates that gas ejection in the manner tested would not produce the desired control forces.

The flow field over the step was very complex during gas ejection and an understanding of the pressure distributions is difficult even when compared with the schlieren photographs. This flow field was further complicated by three dimensional effects and Mach wave interaction. Figures 10 through 22 show how severe the three dimensional losses are at the higher angles of attack.

At the highest angle of attack (13.5 degrees) the pressure distributions for models 1 and 7 indicate erratic flow over the step. This is substantiated by the schlieren motion picture film which shows a boundary layer instability. There is some evidence that this effect is due to a particular combination of leading edge radius and angle of gas ejection; however, the evidence is insufficient to draw a positive conclusion at this time.

The effect of step height on the model pressure distribution is shown in Figures 23 through 26. At small angles of attack, the effect of step height is nearly nonexistent. However, with increasing angle of attack, this effect becomes more apparent. At a 13.5-degree angle of attack, there is an unexplained pressure increase over the front part of the models with decreasing step height. This may be due to a boundary layer feedback, from the ejecting gas, over the forward surface of the model. A pressure increase with decreasing step height is similarly shown over the step and this can be directly attributed to the increased weight flow over the step.

However, figures 23 through 26 are somewhat deceiving since they do not show the full significance of the pressure in the area immediately behind the step. In this area as seen in figure 27 the angle of attack has virtually no bearing on the model pressure. The smaller step is much less efficient in producing a high pressure area immediately behind the step. In the first 10 to 15 percent of the step length from the gas ejection nozzle, the pressure distribution is directly a function of the gas ejection pressure. Beyond this distance from the nozzle, the pressure distribution is relatively independent of the gas ejection pressure, and is more dependent upon the angle of attack.

The effect of leading edge bluntness is shown in figures 28 through 31. As would be expected, the pressure distribution on the forward part of the models has a more negative slope for the blunter model, Model No. 1, than for the sharp L E model, Model No. 2. This holds true for the 0.0, 5.0, 9.5, and 13.5-degree angles of attack tested. The ejecting gas increases the pressure over the step.

The effect of gas ejection angle on the pressure distribution over the step models is shown in figures 32 and 33. Gas ejection parallel to the step gives somewhat higher surface pressures immediately behind the step than does either ejection 10 degrees up or 10 degrees down. This applies for both the larger and smaller step heights; however, the decrease in surface pressure caused by ejecting gas at an angle (rather than parallel) to the step surface is greater for the smaller step heights. Beyond the 10 to 15 percent step length from the gas ejection nozzle, there is little or no effect of gas ejection angle on the pressure distribution over any of the models.

Flat Plate Results

The pressure distribution of the flat plate, Model No. 9, was compared with both theory and experimental data.

The various hypersonic interaction theories compared are:

(1) inviscid theory (ref 3)

$$\left(\frac{p}{p_\infty}\right)_i = 1 + 0.253\, M_\infty^2 \left(\frac{t}{x}\right)^{2/3}$$

(2) linear addition of inviscid theory and viscous theory (ref 3)

$$\left(\frac{p}{p_\infty}\right)_v = 0.92\, \bar{\chi}_\infty - 1$$

or

$$\left(\frac{p}{p_\infty}\right)_i + \left(\frac{p}{p_\infty}\right)_v = 0.253\, M_\infty^2 \left(\frac{t}{x}\right)^{2/3} + 0.92\, \bar{\chi}_\infty$$

(3) Lee's interaction theory (ref 4)

$$p = p_\infty (1 + 0.35\, \bar{\chi}_\infty)$$

(4) Lee's strong interaction theory (ref 4)

$$p = p_\infty (0.92 + 0.52\, \bar{\chi}_\infty)$$

These theories are compared with the HTF test data on figure 34. The correlation is considered good.

The experimental results of Creager, reference 5, for a flat plate similar to the HTF flat plate are shown on figure 35. Test conditions were practically identical to those of the HTF flat plate. Creager's plate, which was 10 times blunter than the HTF plate, showed a pressure distribution very similar in shape and magnitude to the HTF flat plate.

CONCLUSIONS

From the results of this test, the following conclusions are drawn:

1. The flat plate pressure distributions correlate well with established theories and other experimental data.

2. The effects of leading edge bluntness, step height, and ejection angle are small.

3. While the effect of gas ejection is pronounced in the region close to the ejection nozzle it is not sufficient to produce the effect of a physical control surface.

4. Three dimensional losses were pronounced at high angles of attack.

REFERENCES

1. Milling, Robert W., Captain, USAF, The High Temperature Hypersonic Gasdynamics Facility, ASD TN 61-107, September 1961.

2. Crook, Robert T., Calibration of the HTF 5-Inch Conical Nozzle. ASTEA ETR 62-4R, 16 April 1962.

3. Henderson, Arthur Jr., and Johnston, Patrick J., Fluid-Dynamic Properties of Some Simple Sharp and Blunt-Nosed Shapes at Mach Numbers from 16 to 24 in Helium Flow. NASA Memo 5-8-59L, 1959.

4. Schaaf, S.A., Hurlbut, F.C., and Talbot, L., Induced Pressures on Flat Plates in Hypersonic Low Density Flow. ARDC TR 57-47, 1957.

5. Creager, Marcus C., Effects of Leading-Edge Blunting on the Local Heat Transfer and Pressure Distributions over Flat Plates in Supersonic Flow. NACA TN 4142, 1957.

6. Creager, Marcus C., The Effect of Leading-Edge Sweep and Surface Inclination on the Hypersonic Flow Field Over a Blunt Flat Plate, NASA Memo 12-26-58A, 1959.

7. Hammitt, Andrew G., The Hypersonic Viscous Effect on a Flat Plate with Finite Leading Edge. Report No. 378 (WADC TN 57-105), Dept. Aero. Eng., Princeton University, March 1957.

8. Baradell, Donald L., and Bertram, Mitchell, H., The Blunt Plate in Hypersonic Flow. NASA TN D-408, 1960.

APPENDIX I

TABLES

TABLE I

MODELS TESTED

MODEL NUMBER	STEP HEIGHT IN in.	RAMP ANGLE IN degrees	L E RADIUS IN in.	EJECTION SLOT	ANGLE OF EJECTION TO STEP SURFACE IN degrees
1	0.375	—	0.1	Yes	0
2	0.375	—	0.01	Yes	0
3	0.281	—	0.01	Yes	0
4	0.281	—	0.01	Yes	+10
5	0.281	—	0.01	Yes	-10
6	0.187	—	0.01	Yes	0
7	0.187	—	0.01	Yes	+ 10
8	0.093	—	0.01	No	—
9	0.000	0	0.01	No	—
10	—	5	0.01	No	—
11	—	10	0.01	No	—
12	—	20	0.01	No	—
13	—	30	0.01	No	—

TABLE 2

LOCATION OF PRESSURE ORIFICES

ORIFICE NR	x DISTANCE FROM L.E
1	1.250
2	1.625
3	2.000
4	2.375
5	3.250
6	3.500
7	3.750
8	4.000
9	4.250
10	4.500
11	4.750

TABLE 3

SUMMARY OF TEST CONDITIONS

MODEL NUMBER	ANGLE OF ATTACK IN degrees	GAS EJECTION PRESSURE, PSIG	STAGNATION PRESSURE, PSIG	STAGNATION TEMPERATURE, °R
1	-2.0 to 13.5	0 to 122	300 & 600	3610 - 4350
2	-2.0 to 13.5	0 to 130	300 & 600	2270 - 4590
3	0 to 13.5	0 to 130	300	3050 - 3847
4	0 to 13.5	0 to 130	300	3920 - 4480
5	0 to 13.5	0 to 134	300	3970 - 4435
6	0 to 13.5	0 to 130	300	3040 - 3820
7	0 to 13.5	0 to 130	300	3645 - 4350
8	0 to 13.5	0	300	3120 - 4640
9	0 to 13.5	0	300 & 600	3190 - 4580
10	-2.0 to 13.5	0	300 & 600	2465 - 4310
11	0 to 13.5	0	300 & 600	3130 - 4800
12	0 to 13.5	0	300	3000 - 3840
13	0 to 9.4	0	300	3995 - 4310

APPENDIX II

FIGURES

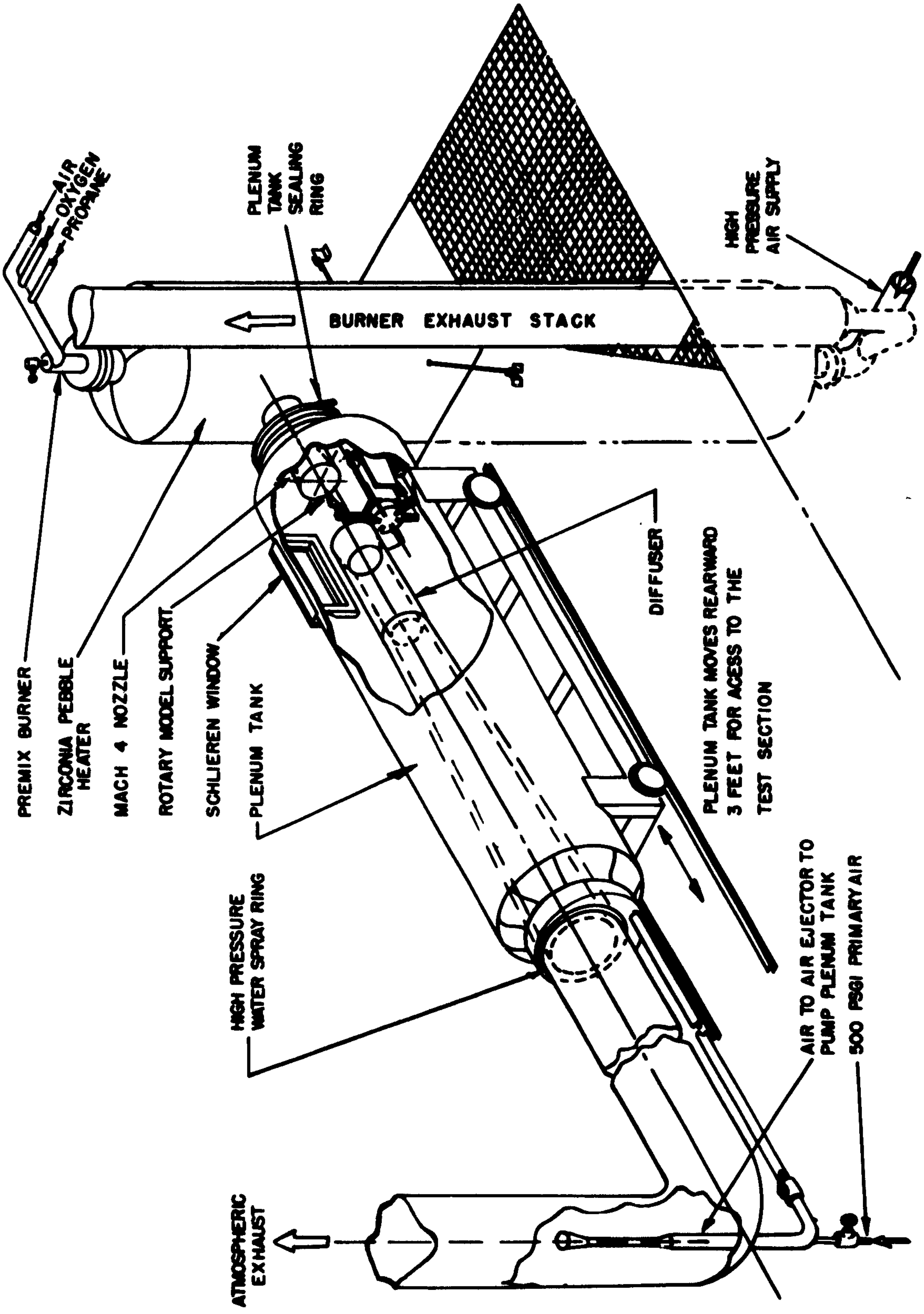

Figure 1. Schematic Layout of the High Temperature Hypersonic Gasdynamic Facility

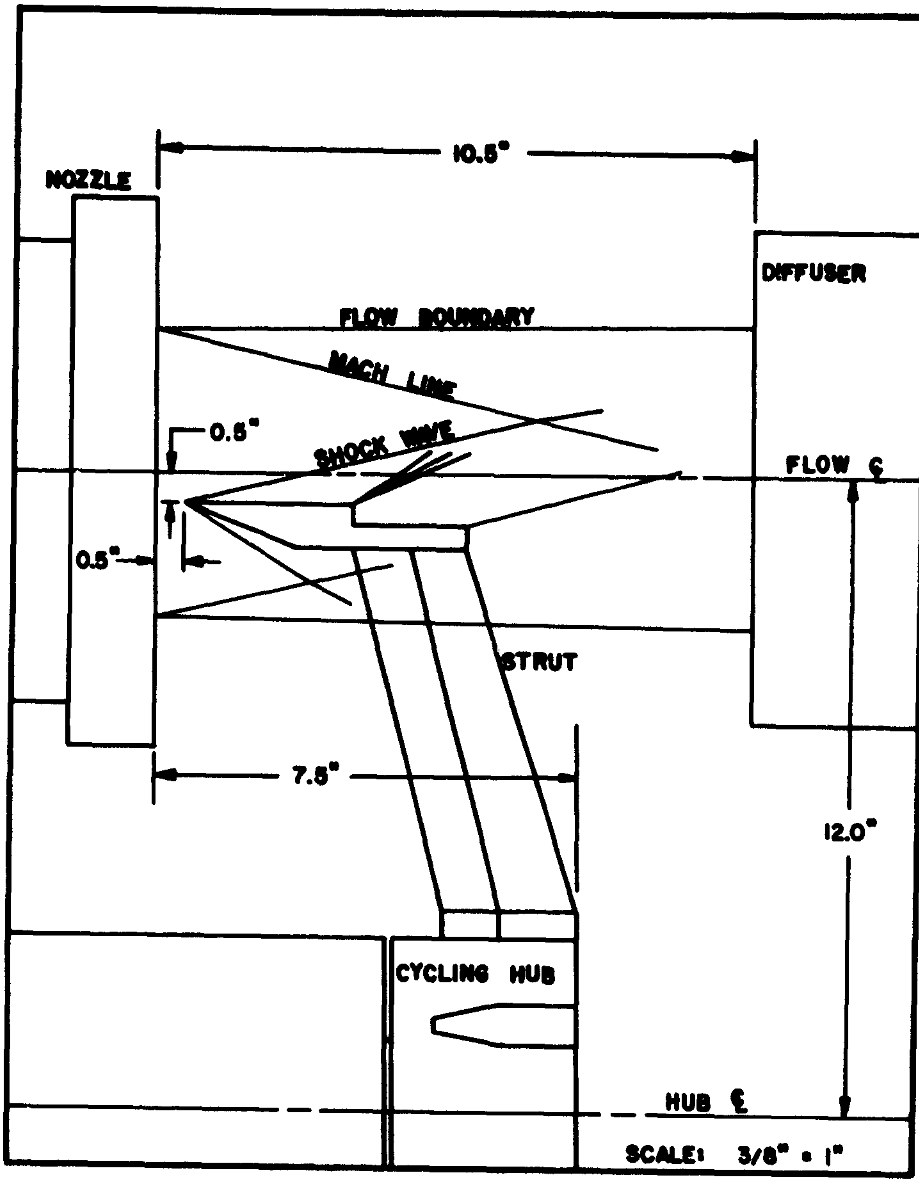

Figure 2. Test Section Arrangement Showing Model Placement

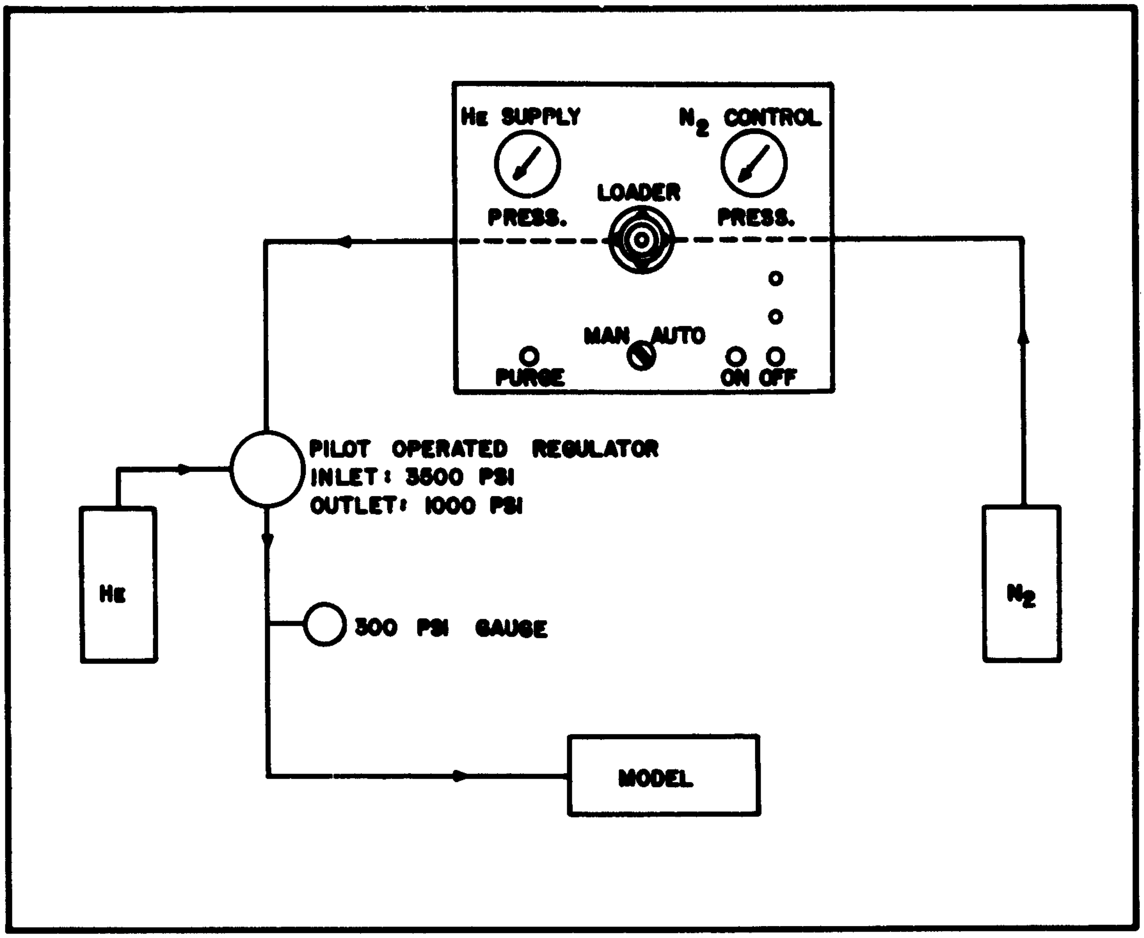

Figure 3. Schematic Layout of the Helium Gas Ejection System

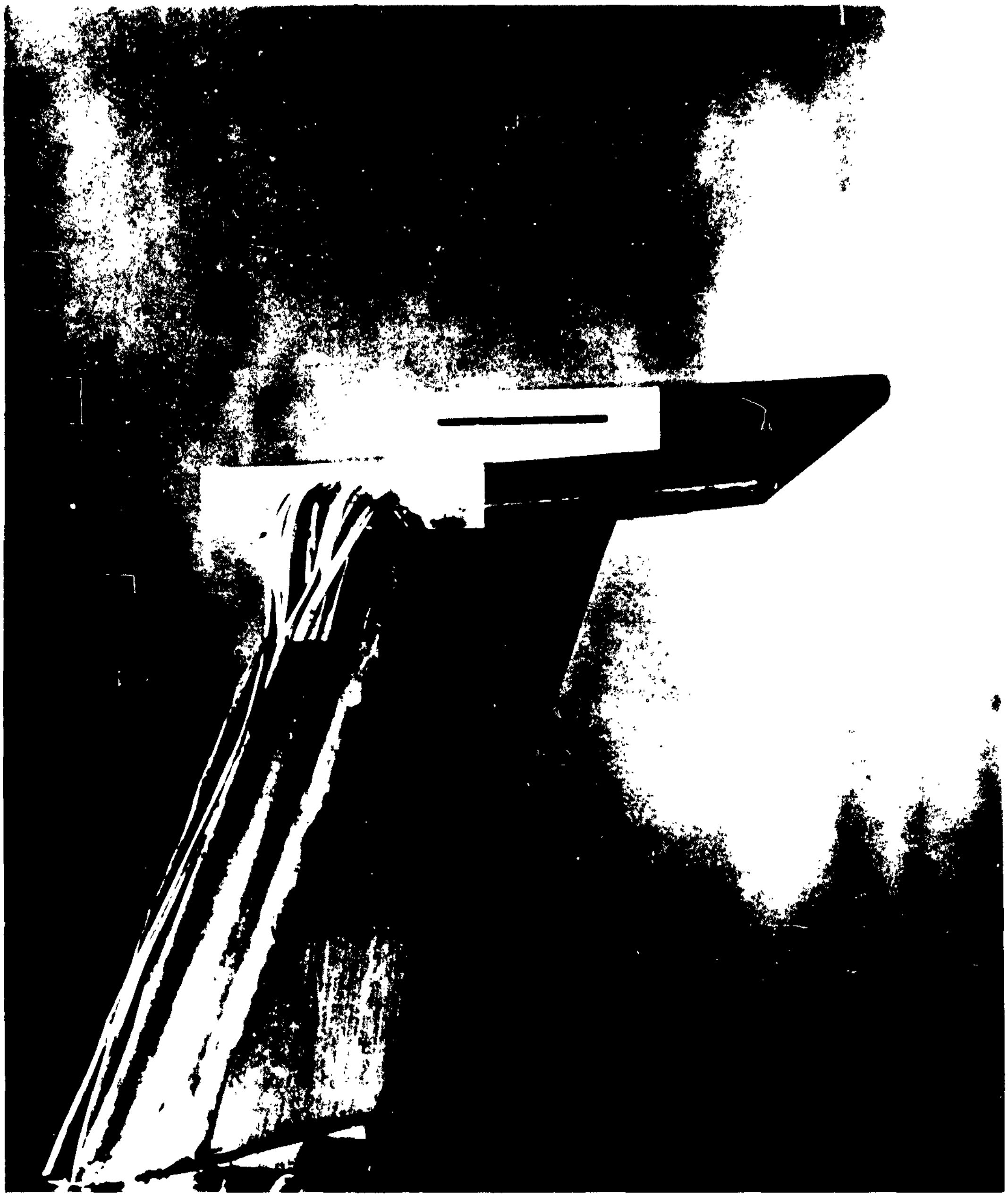

Figure 4. Rear Quarter View of Model No. 1, 0.375 in. Step, 0.1 in. L E Radius

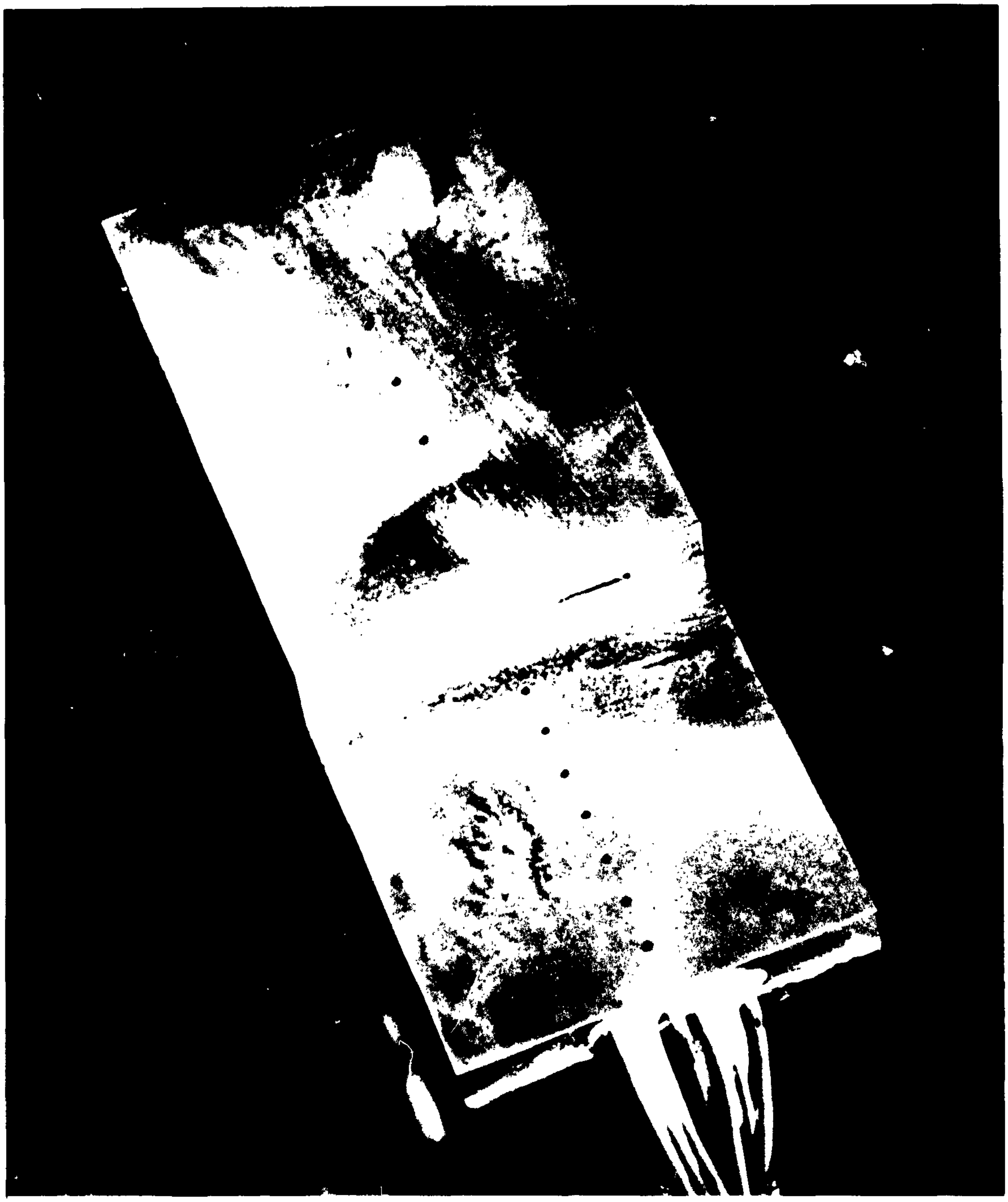

Figure 5. Top View of Model No. 1, Showing Position of Orifices and Gas Ejection Slot on Step Models

Figure 6. Front Quarter View of Model No. 10, 5-degree Ramp, 0.01 in. L E Radius

Figure 7. Top View of Model No. 10, Showing Position of Orifices on Ramp Models

α = 0.0°, $P_J/P_\infty = 0$

α = 0.0°, $P_J/P_\infty = 18$

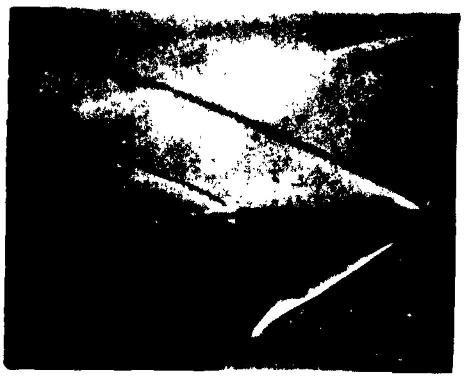

α = 0.0°, $P_J/P_\infty = 34$

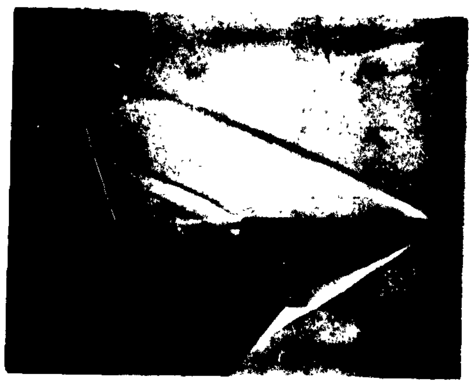

α = 0.0°, $P_J/P_\infty = 51$

Figure 8a. Schlieren Photographs of Model No. 3, P_0 = 313 psia, T_0 = 3,300°R, Re = 1.42×10^6

$\alpha = -5.0°$, $P_J/P_\infty = 0$

$\alpha = -5.0°$, $P_J/P_\infty = 18$

$\alpha = -5.0°$, $P_J/P_\infty = 34$

$\alpha = -5.0°$, $P_J/P_\infty = 51$

Figure 8b. Schlieren Photographs of Model No. 3, P_0 = 313 psia, T_0 = 3,300°R, Re = 1.42×10^6

$\alpha = -9.4$, $P_J/P_\infty = 0$

$\alpha = -9.4°$, $P_J/P_\infty = 18$

$\alpha = -9.4$, $P_J/P_\infty = 51$

Figure 8c. Schlieren Photographs of Model No. 3, $P_o = 313$ psia, $T_o = 3,300°R$, Re = 1.42×10^6

$\alpha = -13.6°$, $P_J/P_\infty = 0$

$\alpha = -13.6°$, $P_J/P_\infty = 18$

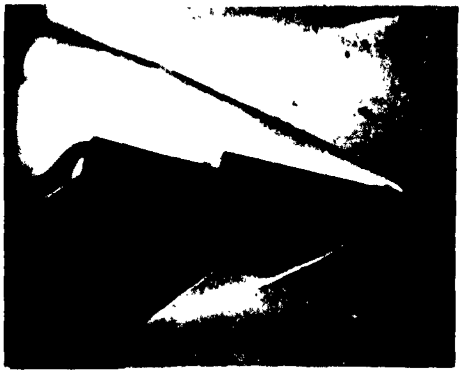

$\alpha = 13.6°$, $P_J/P_\infty = 34$

$\alpha = -13.6°$, $P_J/P_\infty = 51$

Figure 8d. Schlieren Photographs of Model No. 3, P_0 = 313 psia, T_0 = 3,300°R, Re = 1.42×10^6

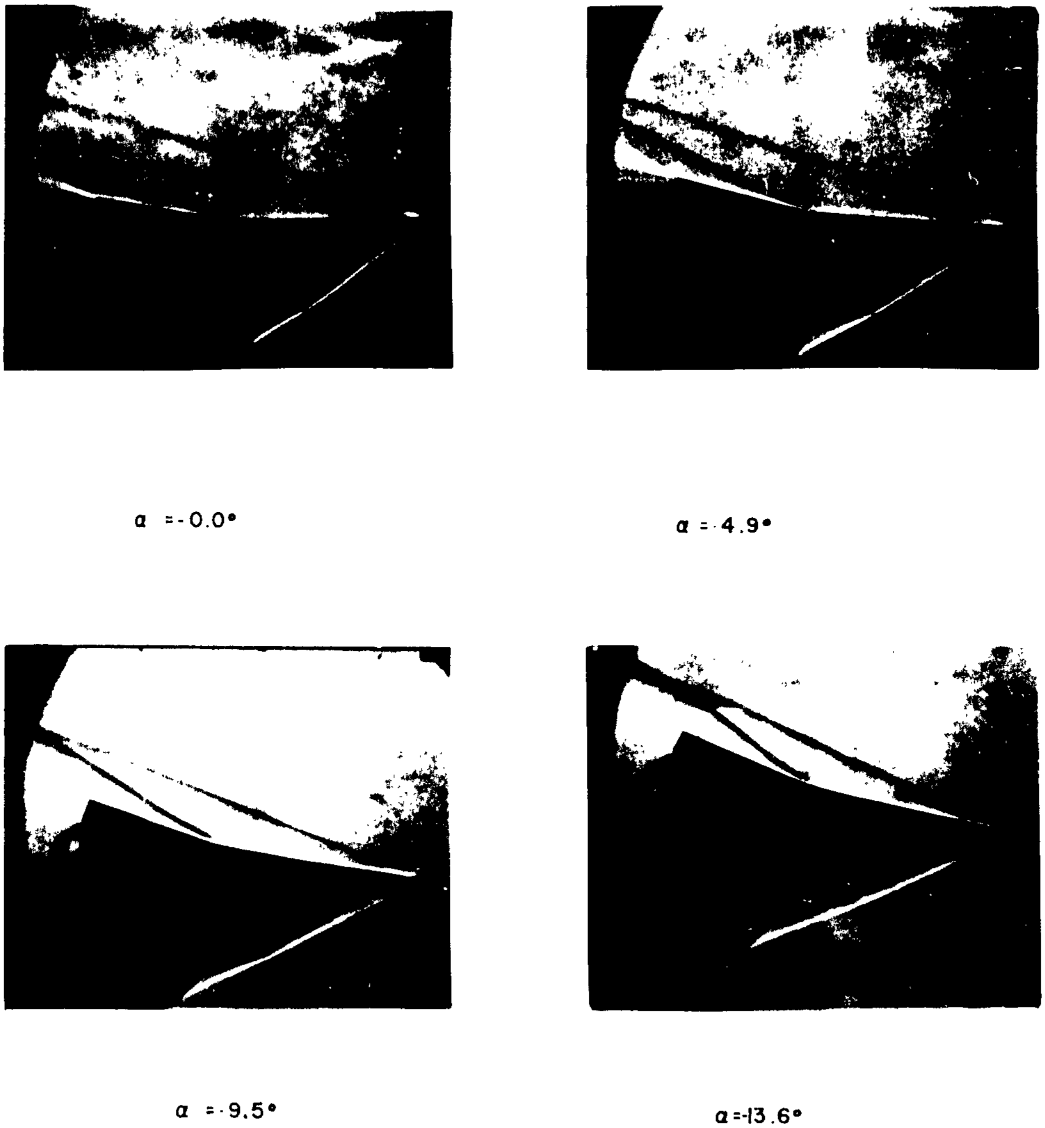

Figure 9. Schlieren Photographs of Model No. 11, P_0 = 315 psia, T_0 = 4,446°R, Re = 0.97 x 10^6

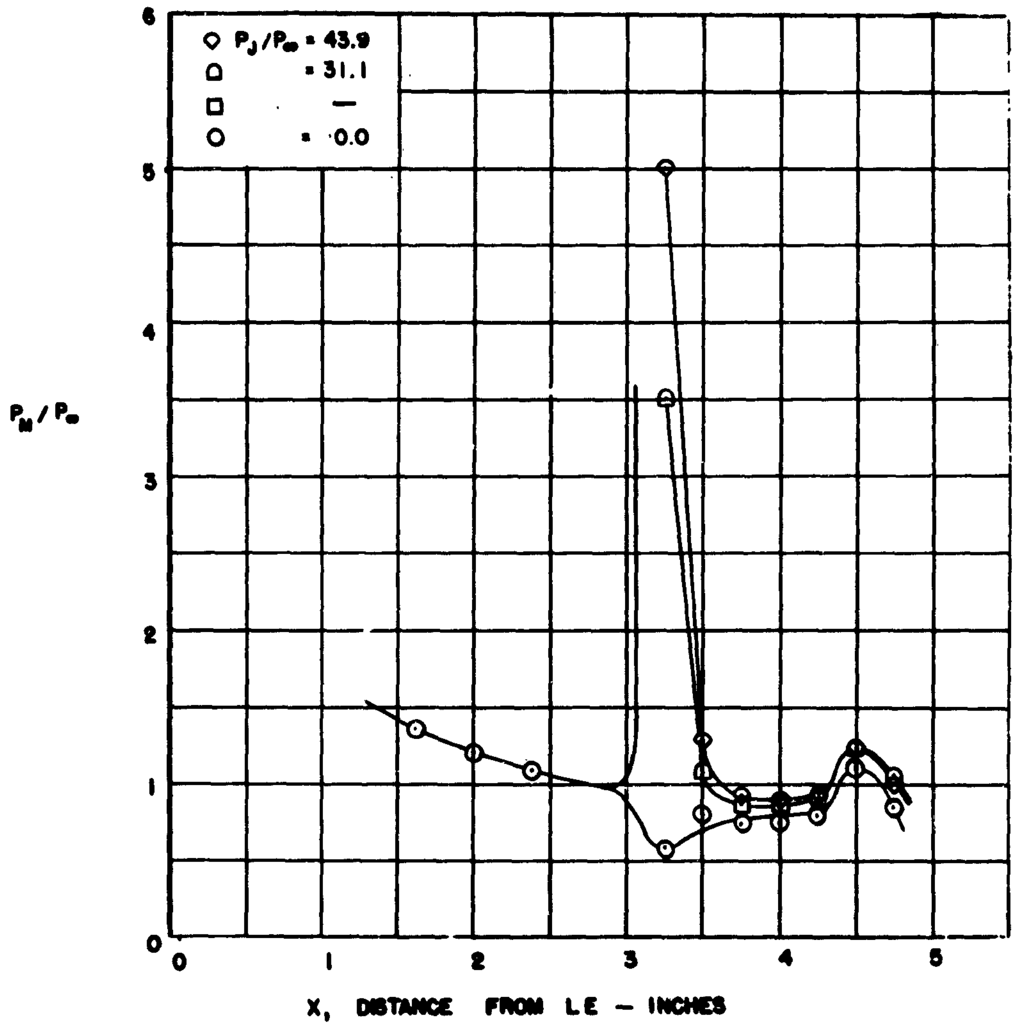

Figure 10a. Pressure Distribution Over Model No. 1 at 0.0-degree Angle of Attack, with Various Gas Ejection Pressures. L E Radius = 0.10 in. Step Height = 0.375 in. P_0 = 312 psia, T_0 = 4,100°R, Re = 1.10×10^6

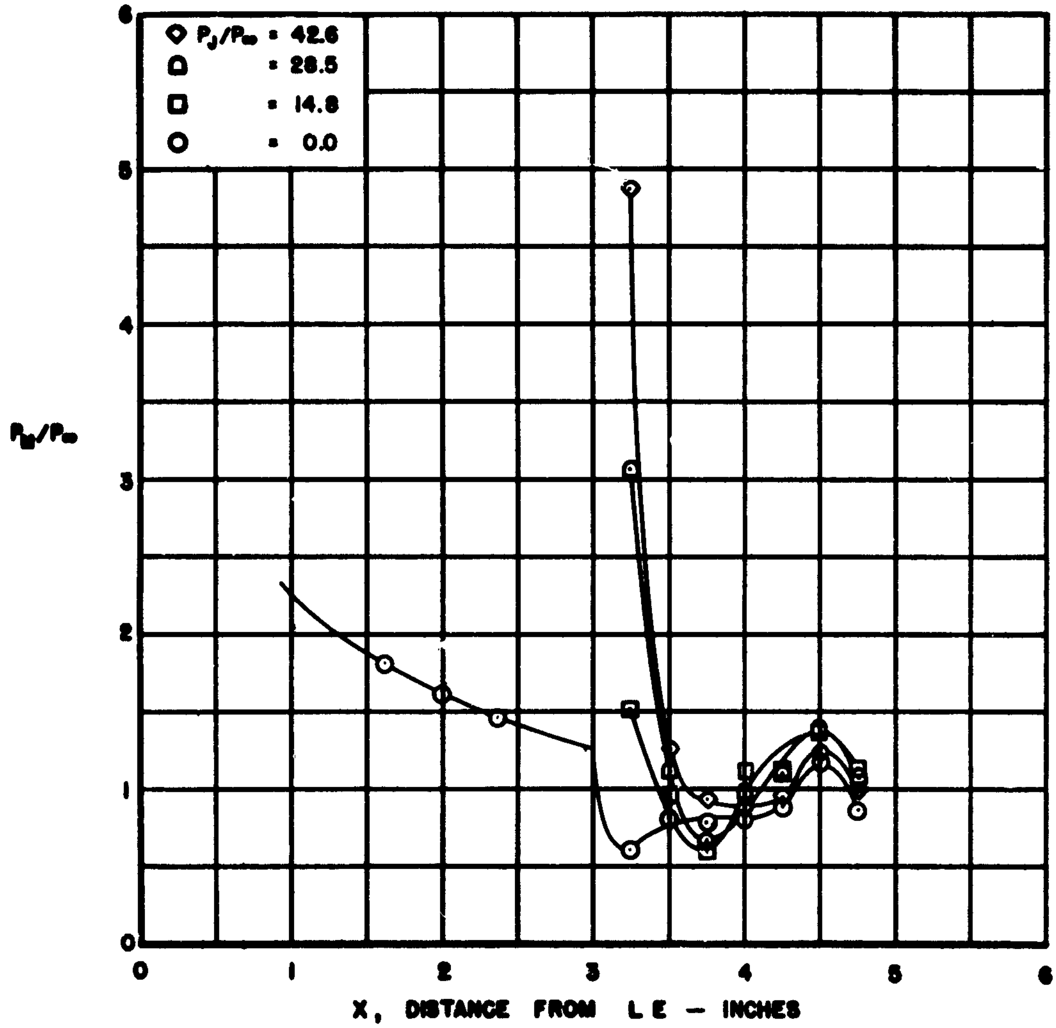

Figure 10b. Pressure Distribution Over Model No. 1 at -4.9-degree Angle of Attack, with Various Gas Ejection Pressures. L E Radius = 0.10 in., Step Height = 0.375 in. P_0 = 312 psia, T_0 = 4,100°R, Re = 1.10 x 10^6

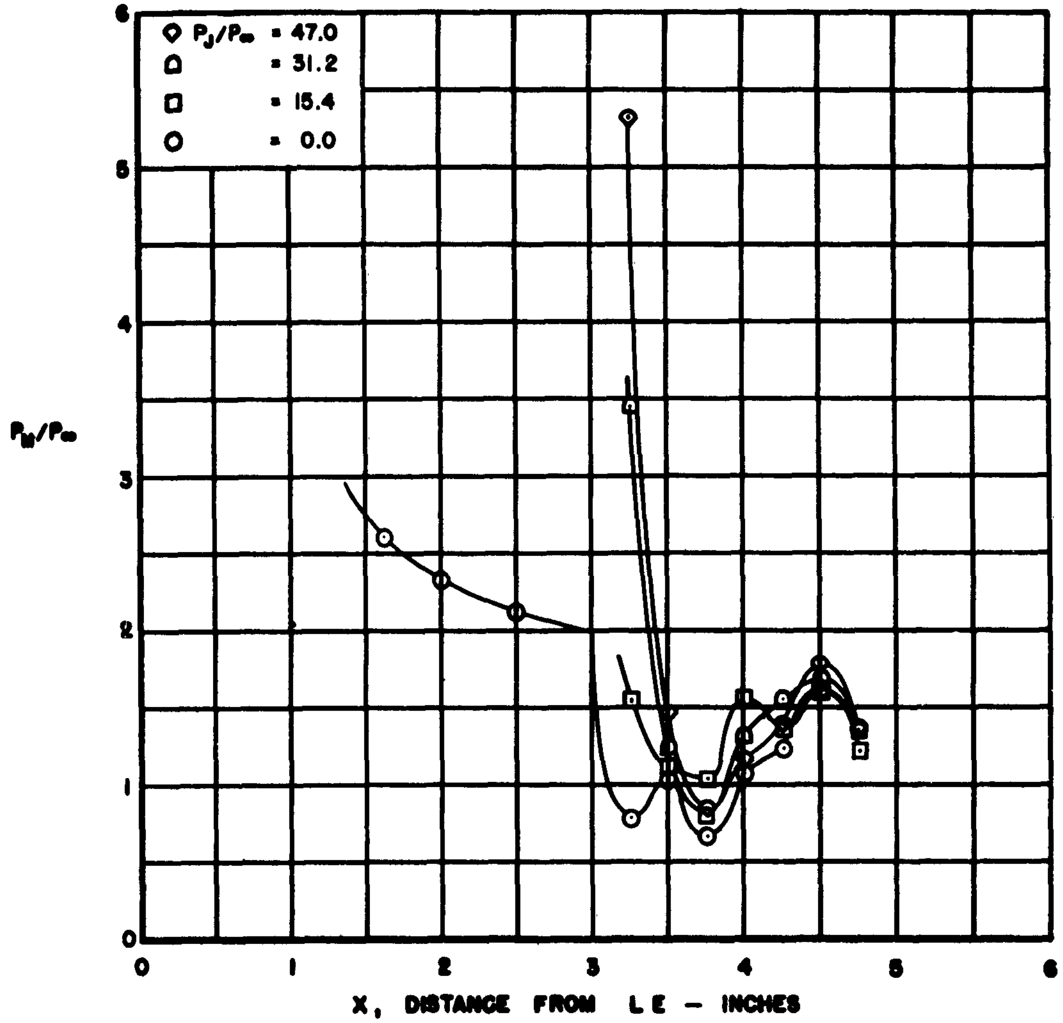

Figure 10c. **Pressure Distribution Over Model No. 1 at -9.4-degree Angle of Attack, with Various Gas Ejection Pressures. L E Radius = 0.10 in., Step Height = 0.375 in. P_0 = 312 psia, T_0 = 4,100°R, Re = 1.10 x 10^6**

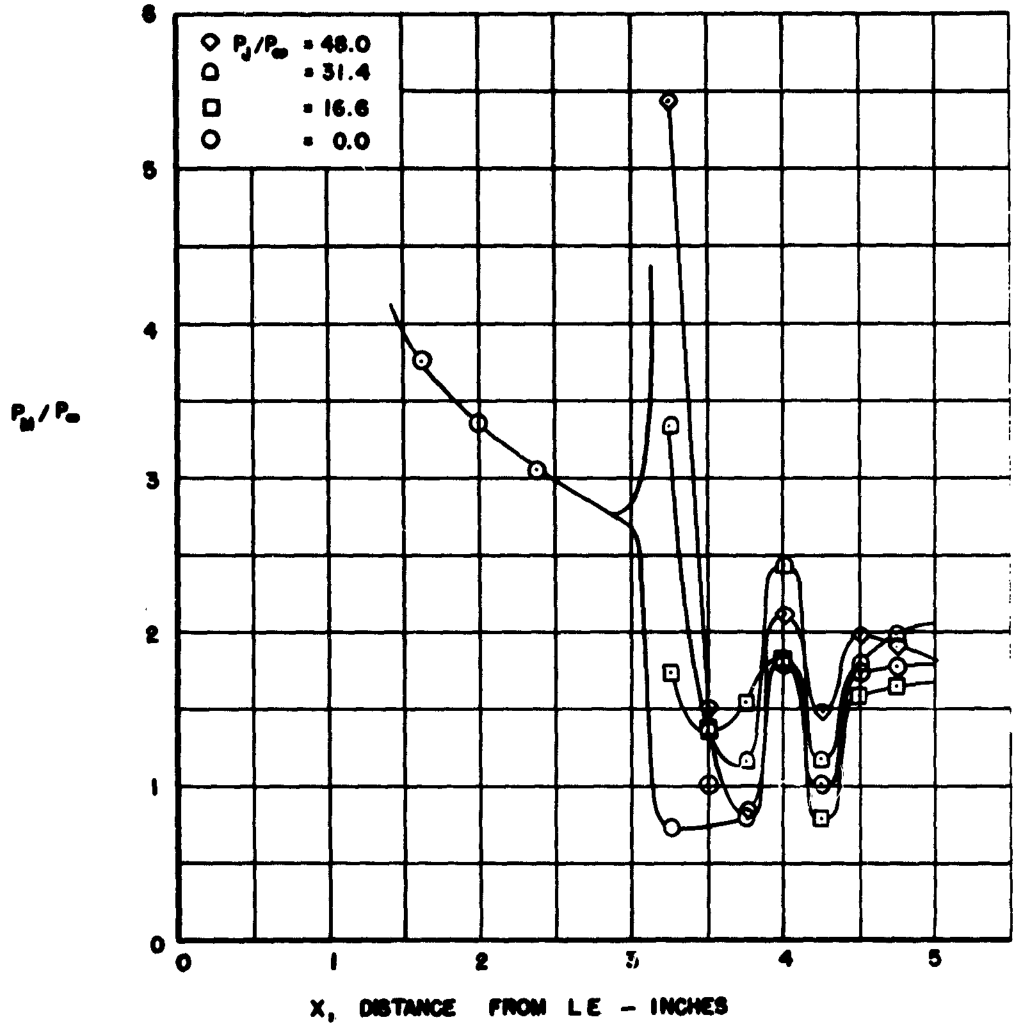

Figure 10d. Pressure Distribution Over Model No. 1 at -13.5-degree Angle of Attack, with Various Gas Ejection Pressures. L E Radius = 0.10 in., Step Height = 0.375 in., P_0 = 312 psia, T_0 = 4,100°R, Re = 0.10 x 10^6

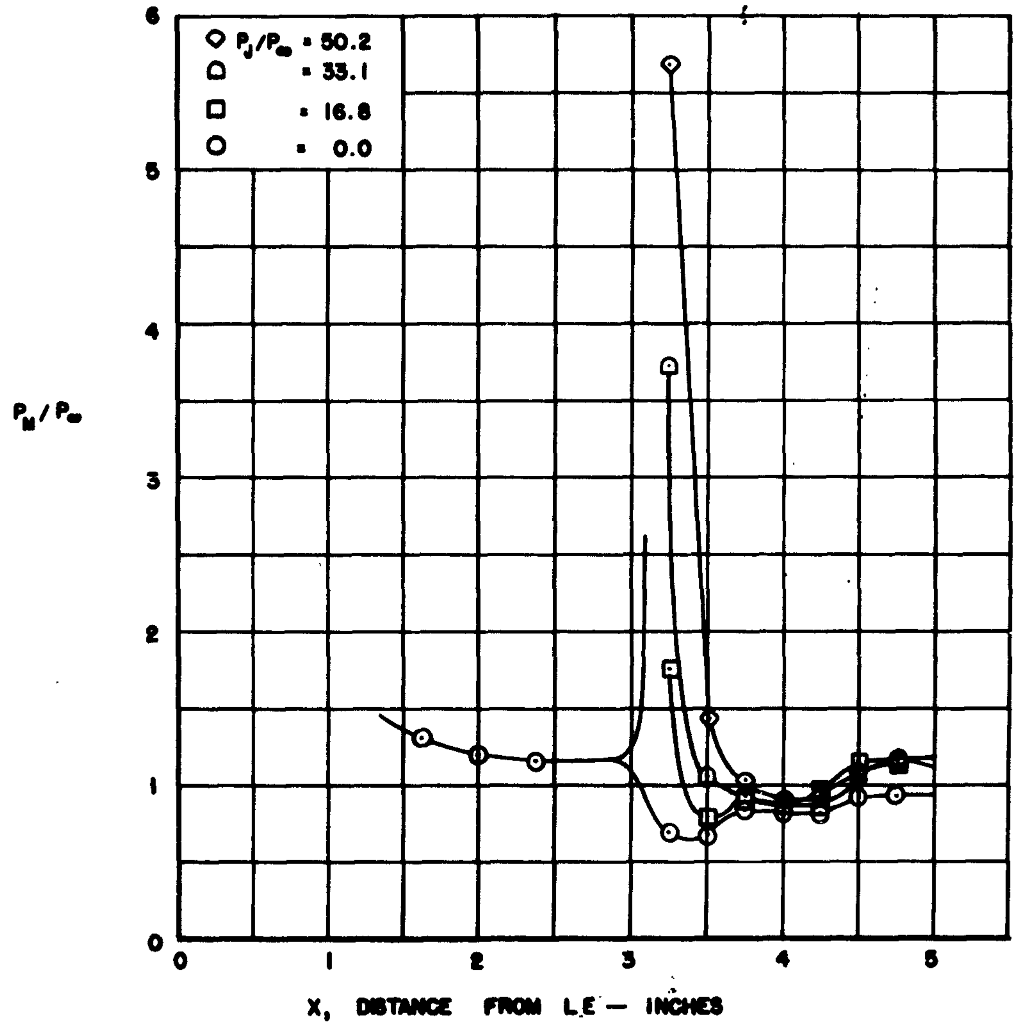

Figure 11a. Pressure Distribution Over Model No. 2 at 0.0-degree Angle of Attack, with Various Gas Ejection Pressures. L E Radius = 0.01 in., Step Height = 0.375 in. P_0 = 312 psia, T_0 = 4,100°R, Re = 1.09×10^6

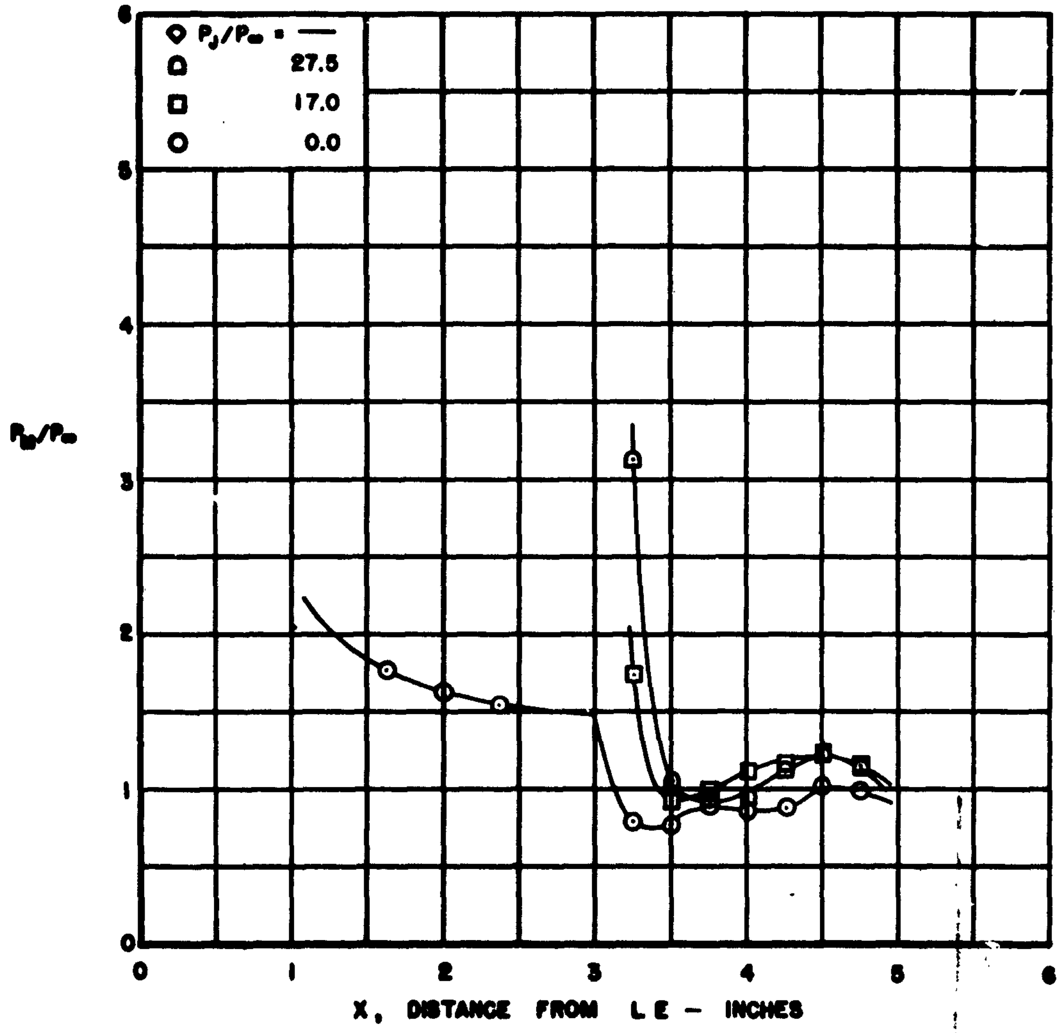

Figure 11b. Pressure Distribution Over Model No. 2 at -5.0-degree Angle of Attack with Various Gas Ejection Pressures. L E Radius = 0.01 in., Step Height = 0.375 in. P_0 = 312 psia, T_0 = 4,100°R, Re = 1.09 x 10^6

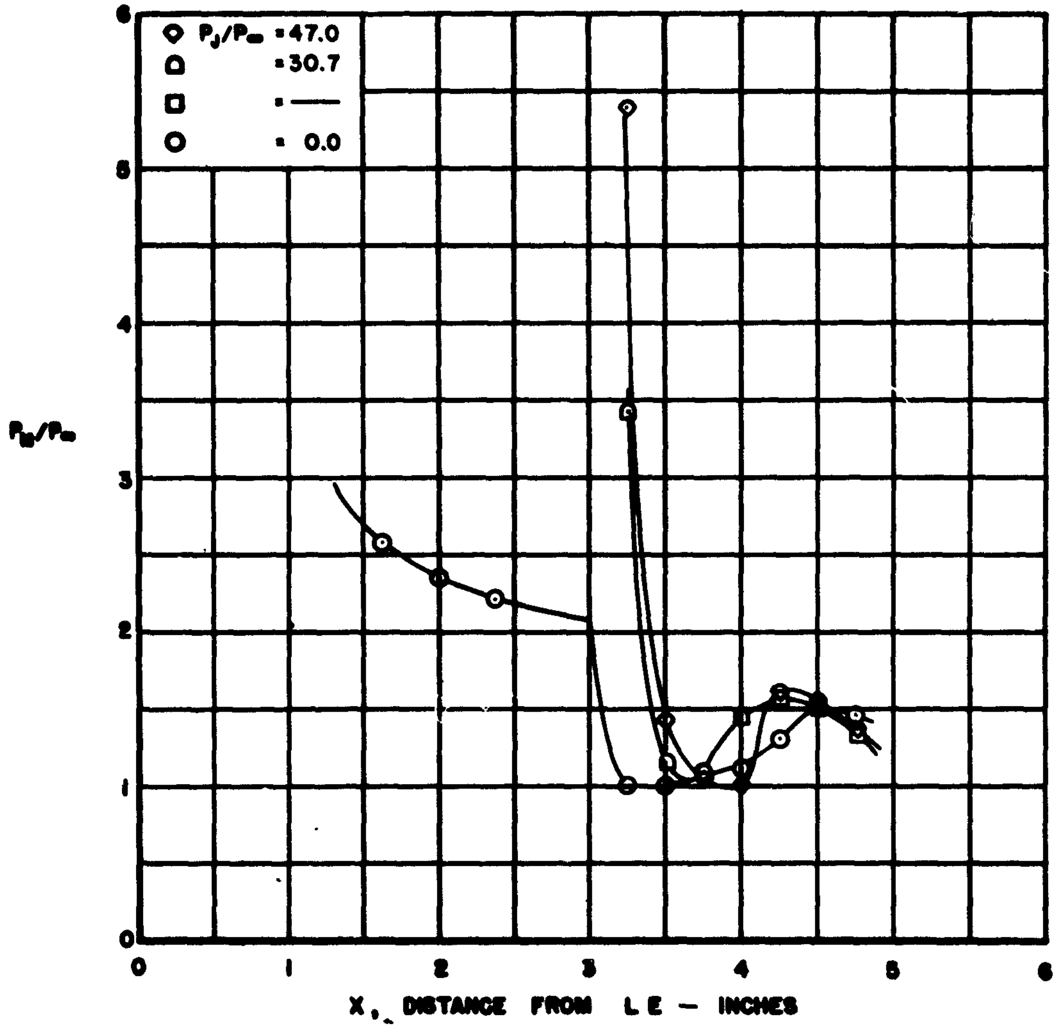

Figure 11c. Pressure Distribution Over Model 2 at -9.5-degree Angle of Attack with Various Gas Ejection Pressures. L E Radius = 0.01 in., Step Height = 0.375 in., P_0 = 312 psia, T_0 = 4,100°R, Re = 1.09 x 10^6

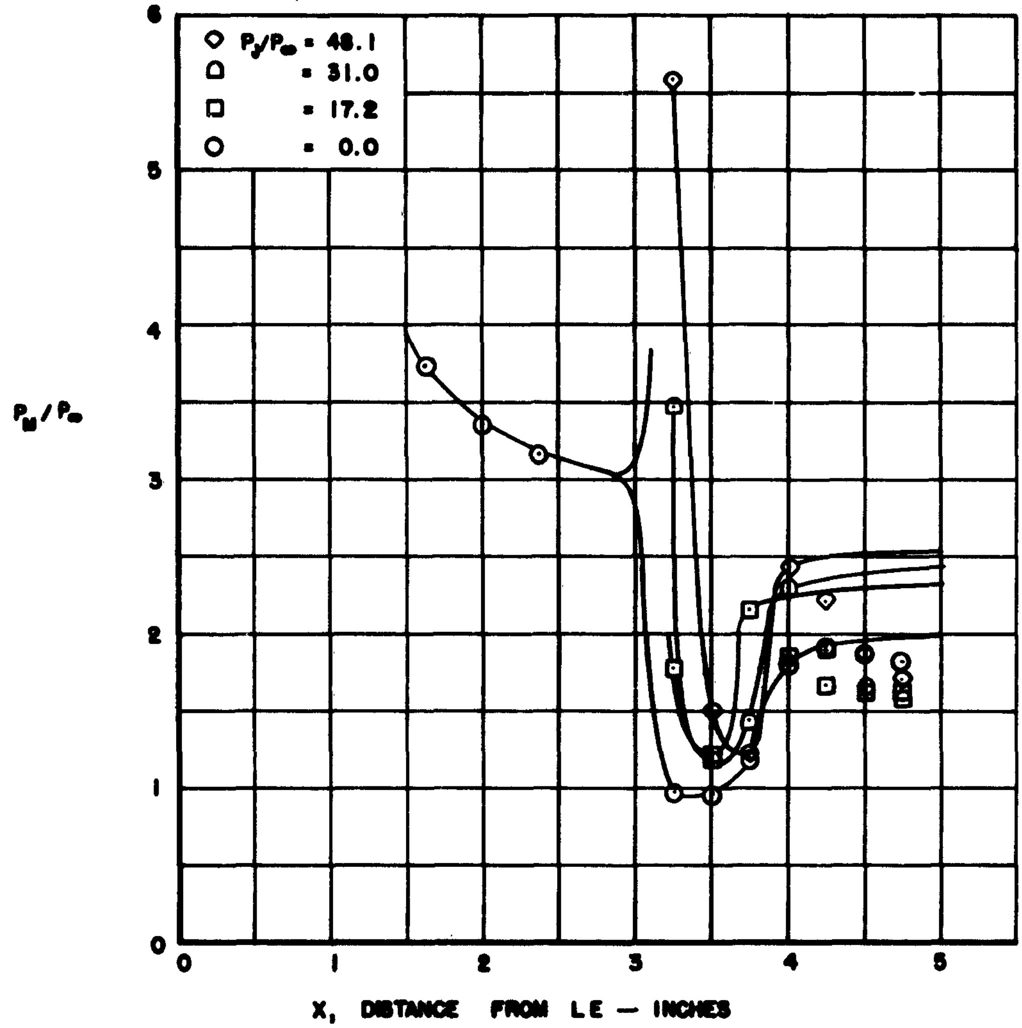

Figure 11d. Pressure Distribution Over Model 2 at -13.6-degree Angle of Attack with Various Gas Ejection Pressures. L E Radius = 0.01 in., Step Height = 0.375, P_0 = 312 psia, T_0 = 4,100°R, Re = 1.09 x 10^6

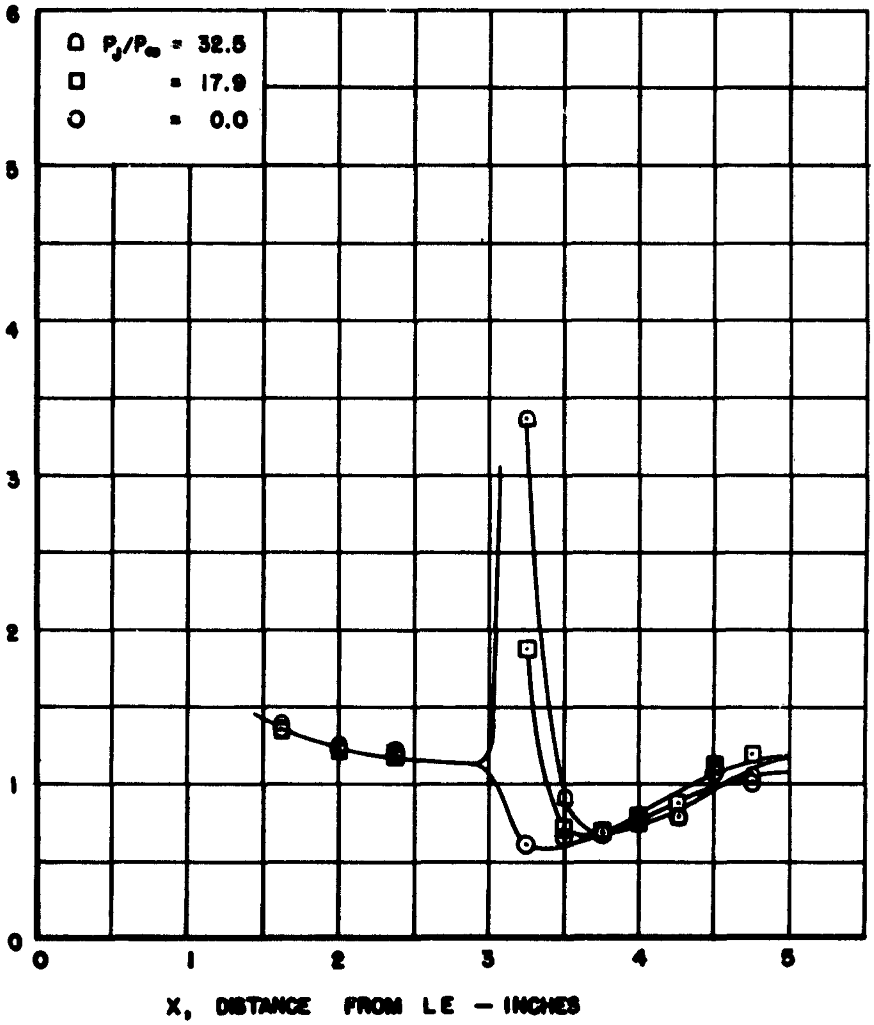

Figure 12a. Pressure Distribution Over Model No. 3 at 0.0-degree Angle of Attack with Various Gas Ejection Pressures. L E Radius = 0.01 in., Step Height = 0.281 in., P_0 = 313 psia, T_0 = 3,300°R, Re = 1.42 x 10^6

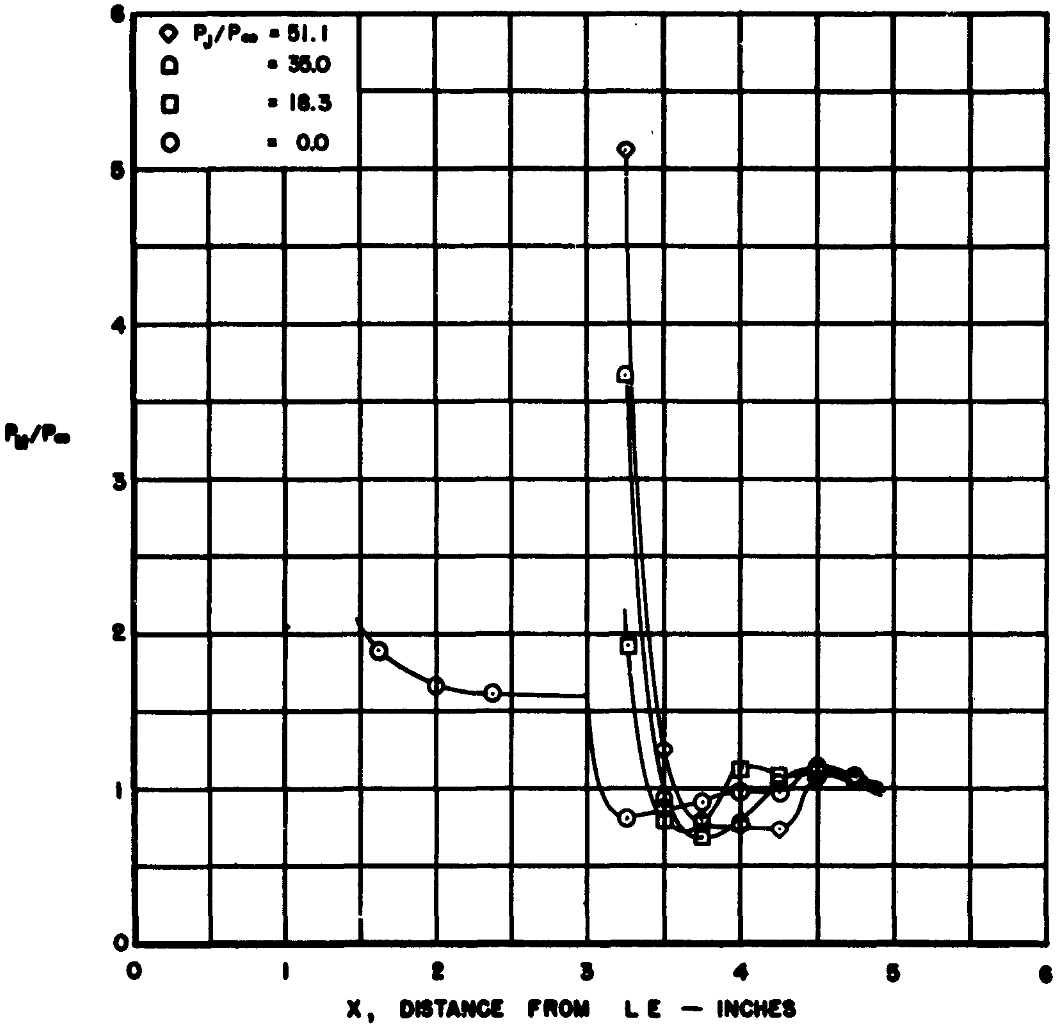

Figure 12b. Pressure Distribution Over Model No. 3 at -5.0-degree Angle of Attack with Various Gas Ejection Pressures. L E Radius = 0.01 in., Step Height = 0.281 in., P_0 = 313 psia, T_0 = 3,300°R, Re = 1.42×10^6

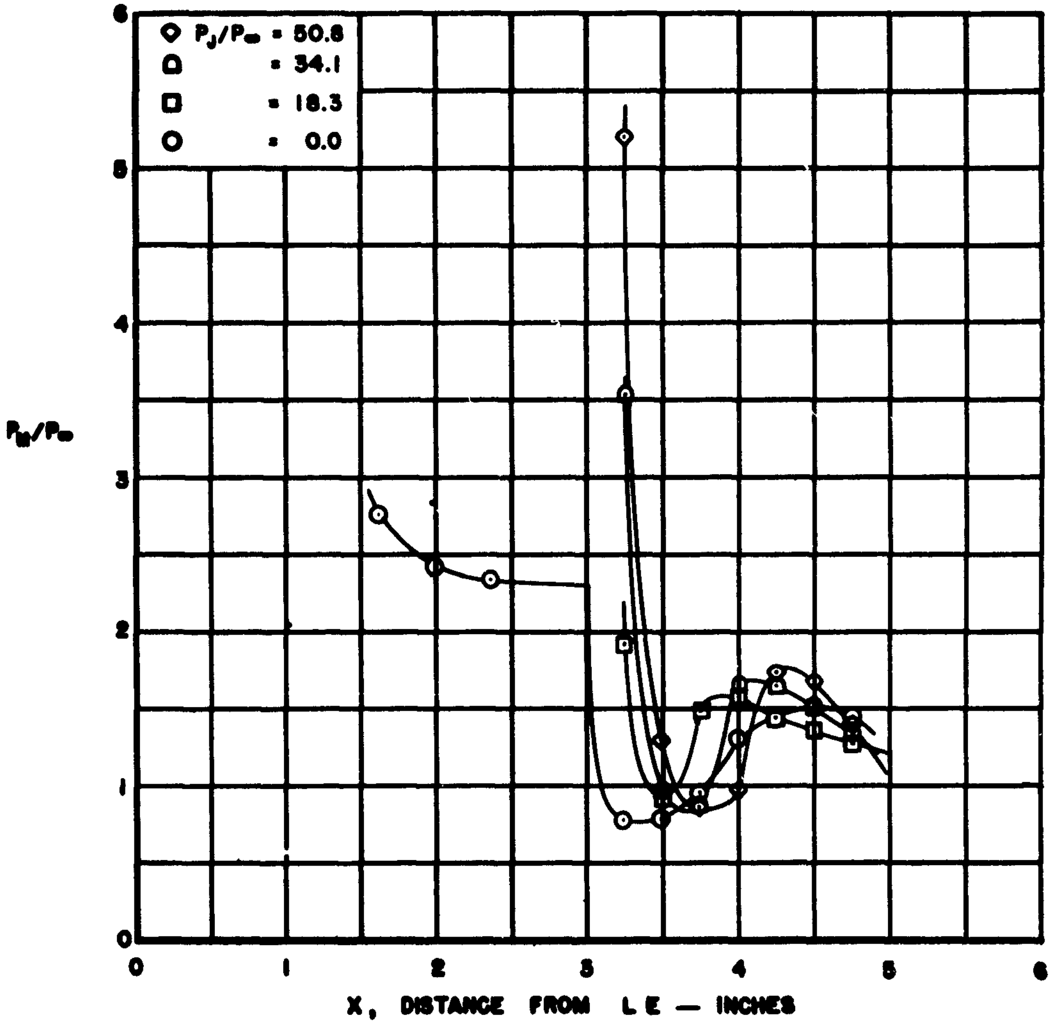

Figure 12c. Pressure Distribution Over Model No. 3 at -9.4-degree Angle of Attack with Various Gas Ejection Pressures. L E Radius = 0.01 in., Step Height = 0.281 in., P_0 = 313 psia, T_0 = 3,300°R, Re = 1.42×10^6

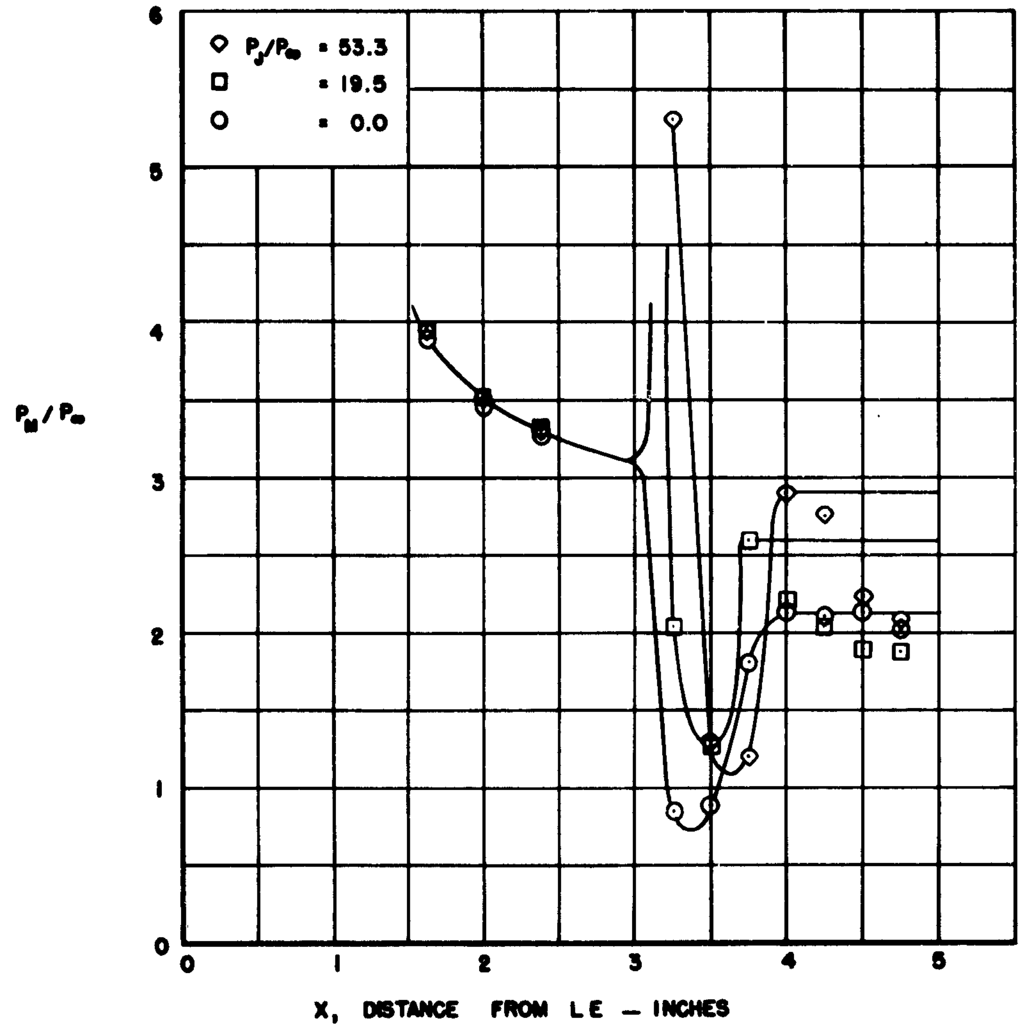

Figure 12d. Pressure Distribution Over Model No. 3 at -13.6-degree Angle of Attack with Various Gas Ejection Pressures. L E Radius = 0.01 in., Step Height = 0.281 in., P_0 = 313 psia, T_0 = 3,300°R, Re = 1.42 x 10^6

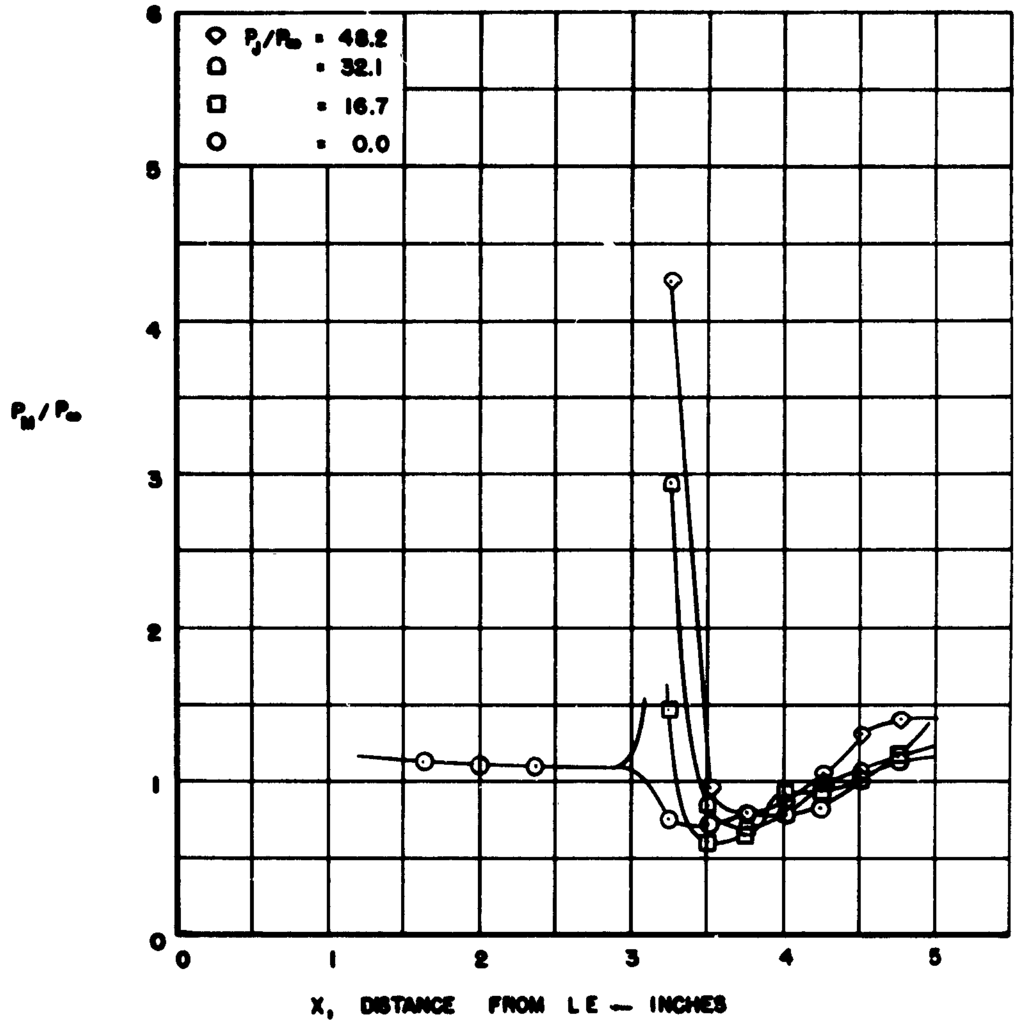

Figure 13a. Pressure Distribution Over Model No. 4 at 0.0-degree Angle of Attack with Various Gas Ejection Pressures. L E Radius = 0.01 in., Step Height = 0.281 in. Ejection 10 degrees Up. P_0 = 313 psia, T_0 = 4,200°R, Re = 1.09×10^6

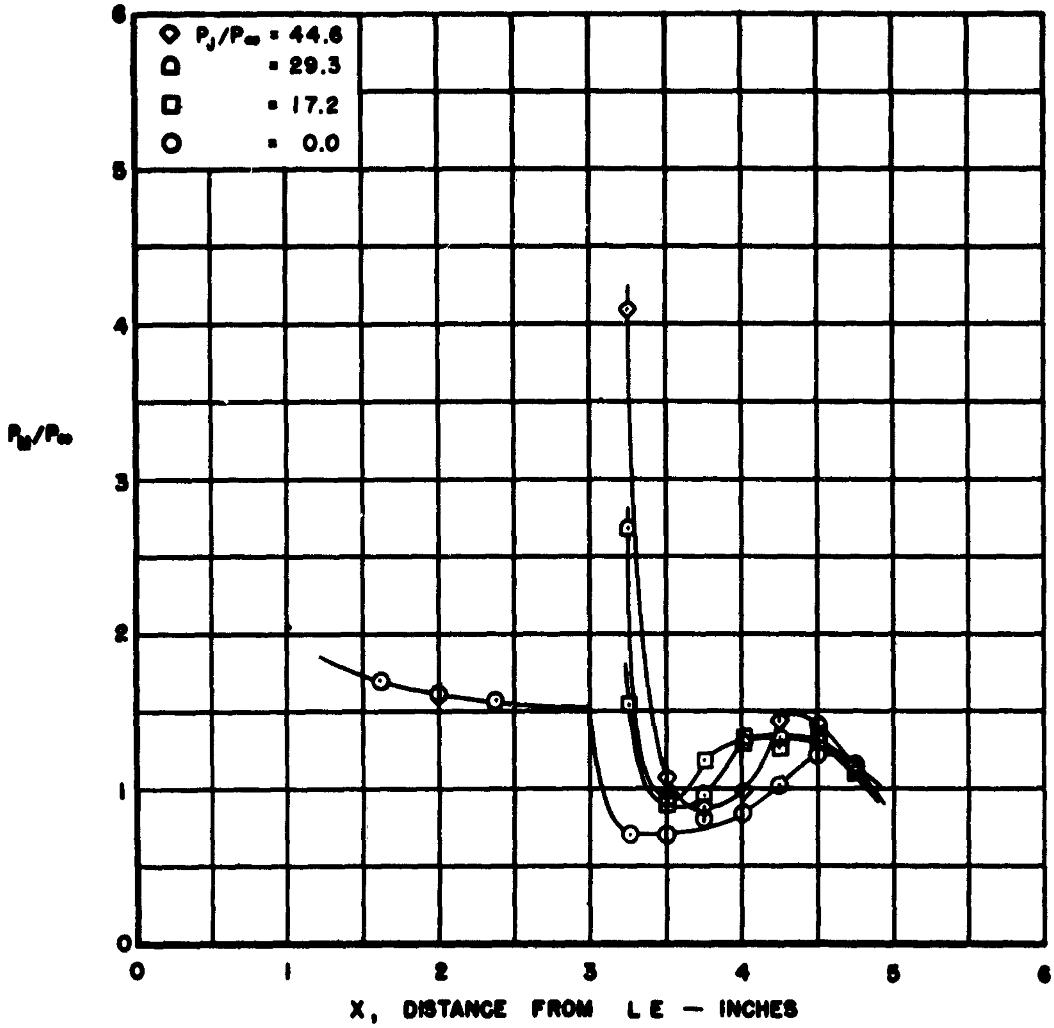

Figure 13b. Pressure Distribution Over Model No. 4 at -5.0-degree Angle of Attack with Various Gas Ejection Pressures. L E Radius = 0.01 in., Step Height = 0.281 in. Ejection 10 degrees Up. P_0 = 313 psia, T_0 = 4,200°R, Re = 1.09×10^6

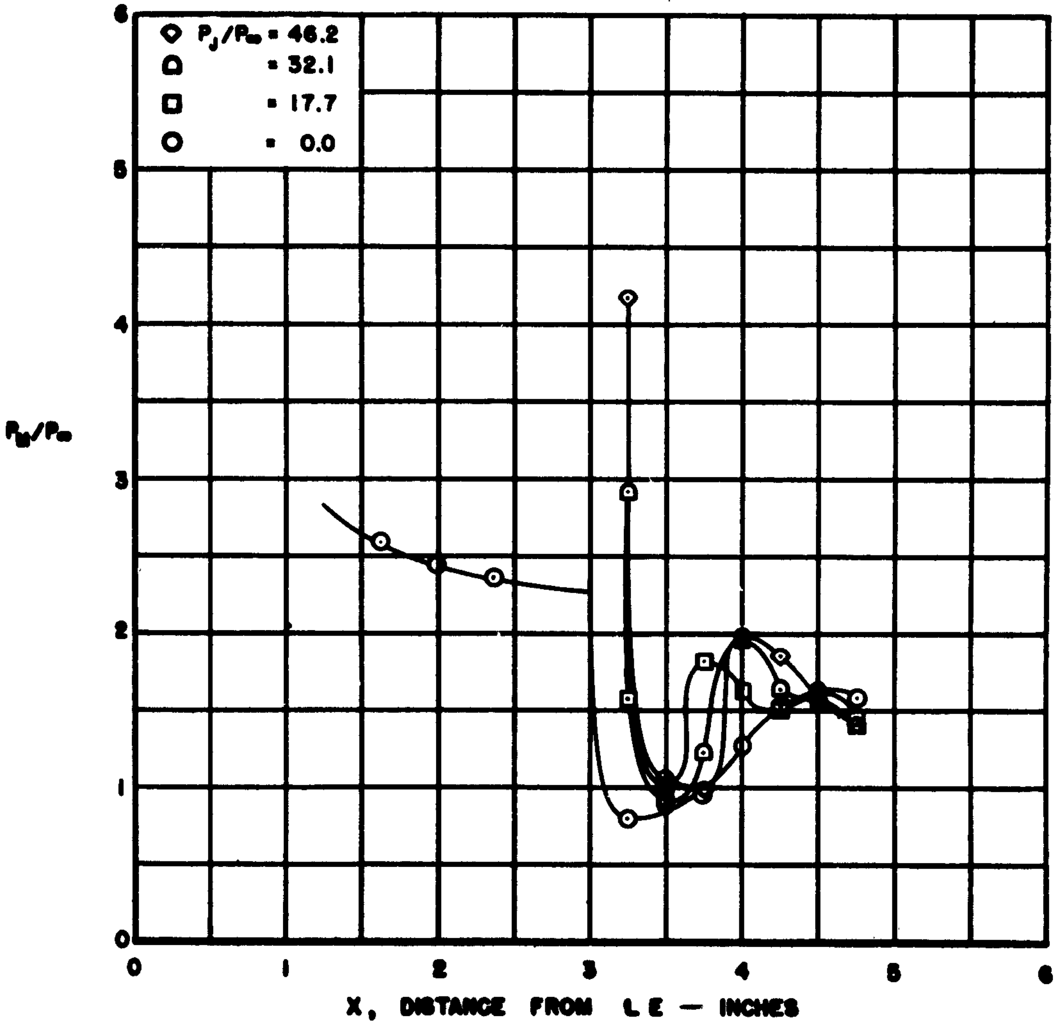

Figure 13c. Pressure Distribution Over Model No. 4 at -9.5-degree Angle of Attack with Various Gas Ejection Pressures. L E Radius = 0.01 in., Step Height = 0.281 in. Ejection 10 degrees Up. P_0 = 313 psia, T_0 = 4,200°R, Re = 1.09×10^6

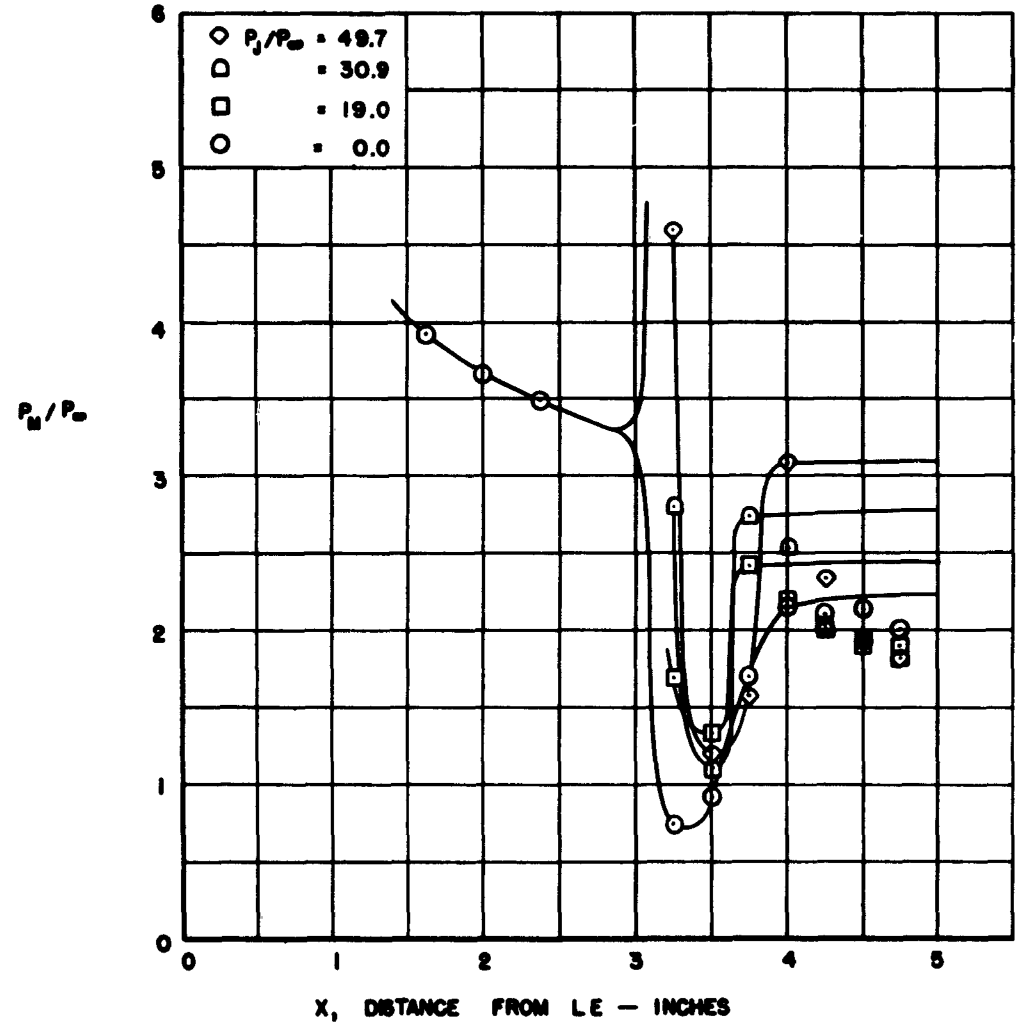

Figure 13d. Pressure Distribution Over Model No. 4 at -13.6-degree Angle of Attack with Various Gas Ejection Pressures. L E Radius = 0.01 in., Step Height = 0.281 in. Ejection 10 degrees Up. P_0 = 313 psia, T_0 = 4,200°R, Re = 1.09×10^6

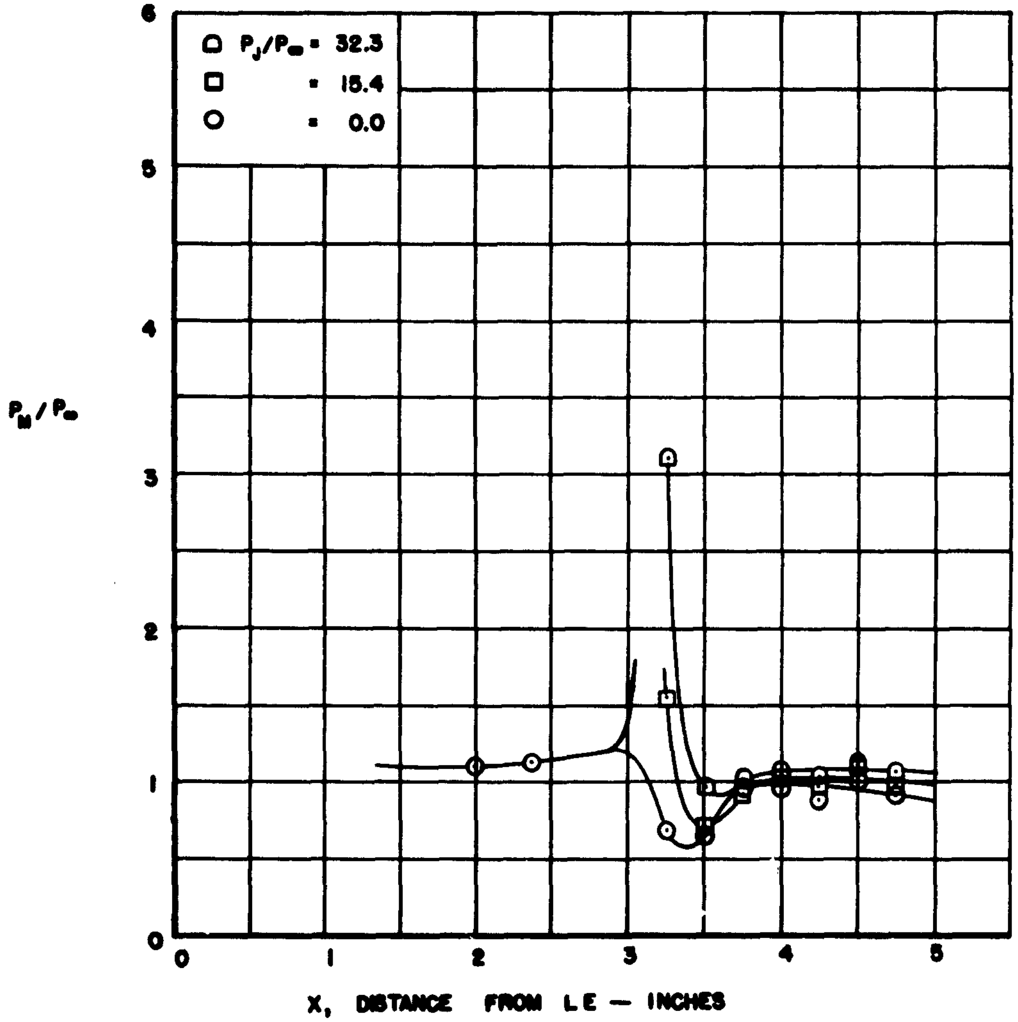

Figure 14a. Pressure Distribution Over Model No. 5 at 0.0-degree Angle of Attack with Various Gas Ejection Pressures. L E Radius = 0.01 in., Step Height = 0.281 in., Ejection 10 degrees Down. P_0 = 313 psia, T_0 = 4,200°R, Re = 1.02×10^6

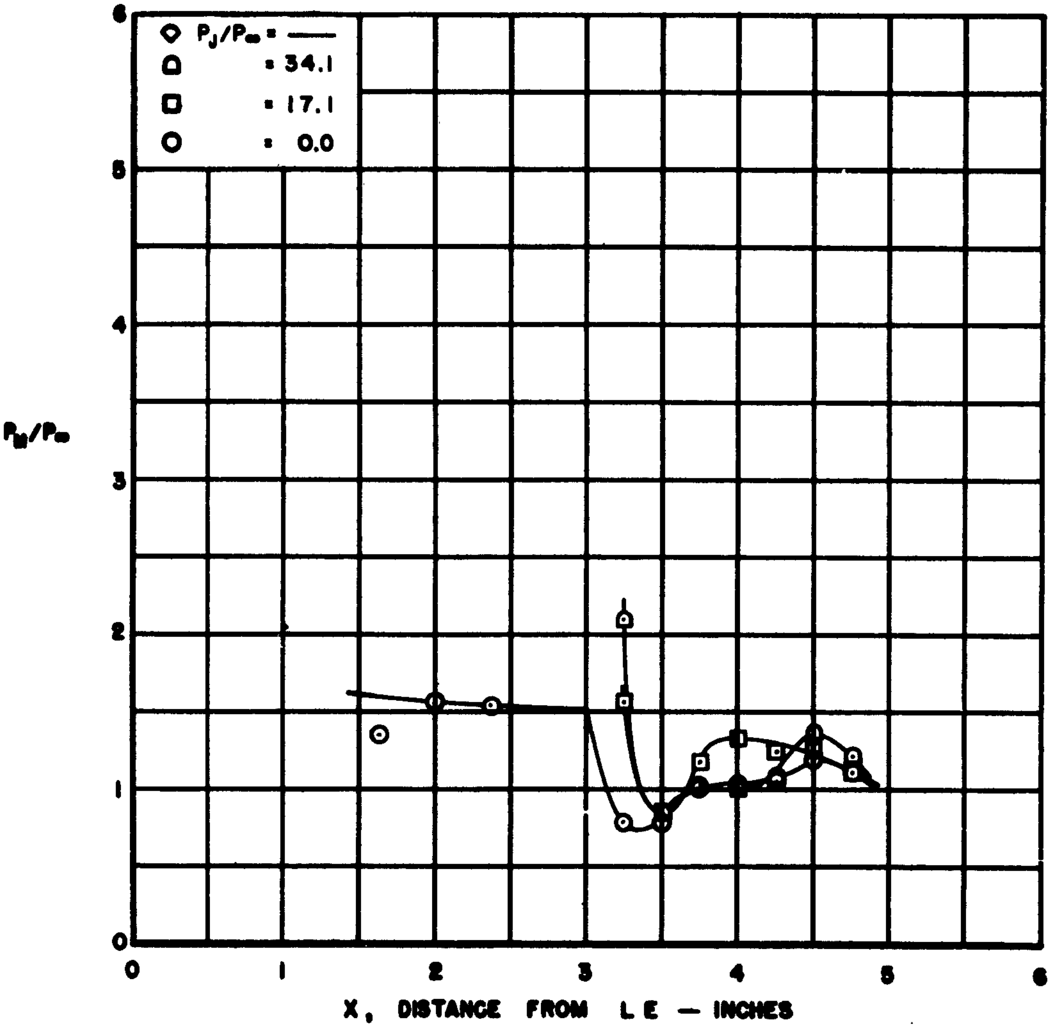

Figure 14b. Pressure Distribution Over Model No. 5 at -4.9-degree Angle of Attack with Various Gas Ejection Pressures. L E Radius = 0.01 in., Step Height = 0.281 in., Ejection 10 degrees Down. P_0 = 313 psia, T_0 = 4,200°R, Re = 1.02×10^6

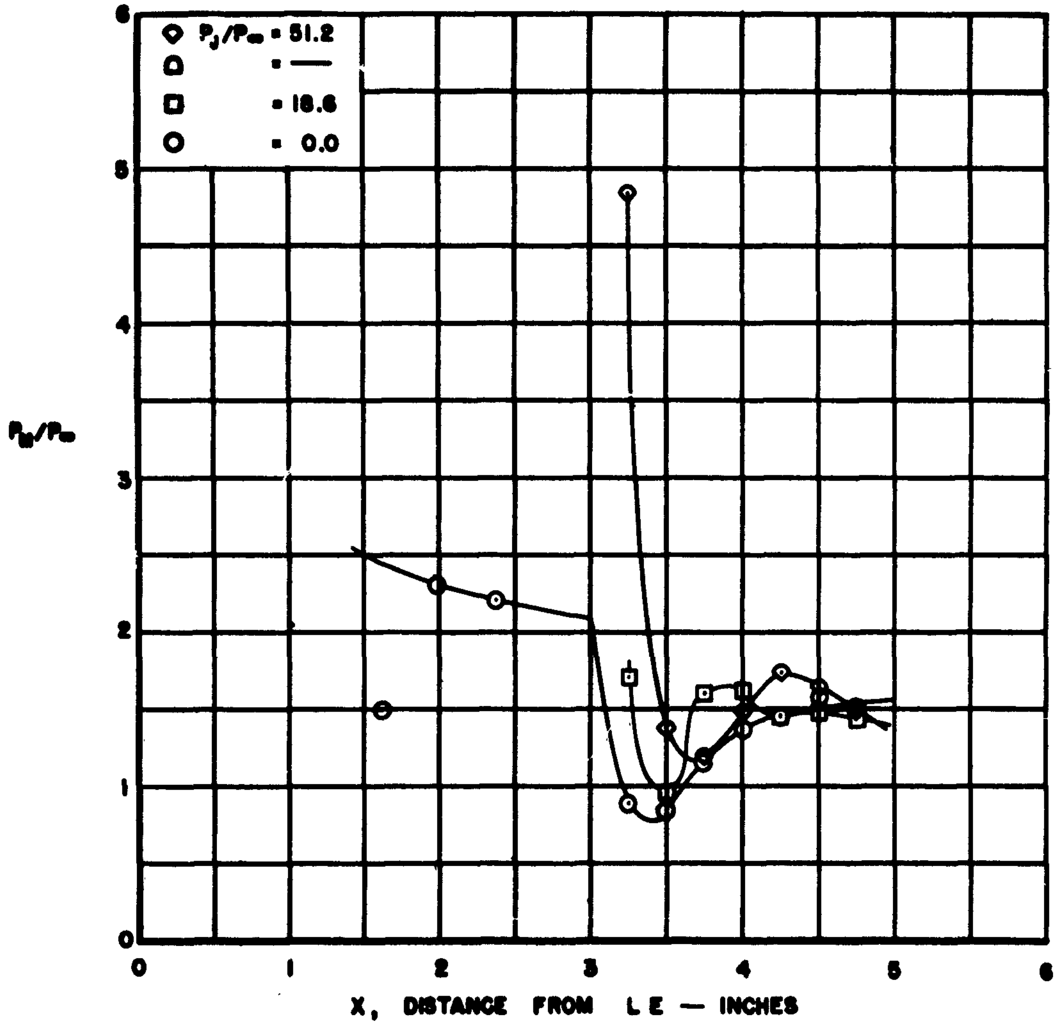

Figure 14c. Pressure Distribution Over Model No. 5 at -9.5-degree Angle of Attack with Various Gas Ejection Pressures. L E Radius = 0.01 in., Step Height = 0.281 in., Ejection 10 degrees Down. P_0 = 313 psia, T_0 = 4,200°R, Re = 1.02×10^6

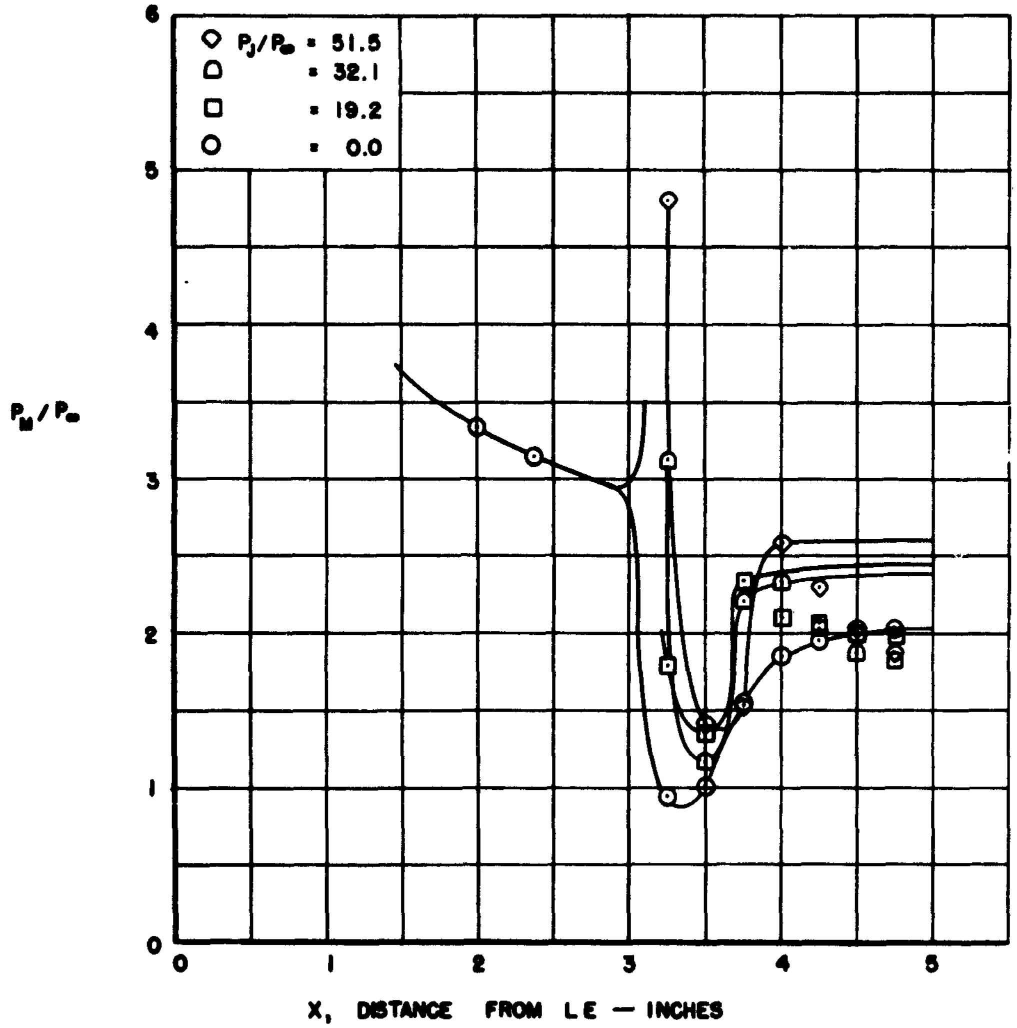

Figure 14d. Pressure Distribution Over Model No. 5 at -13.6-degree Angle of Attack with Various Gas Ejection Pressures. L E Radius = 0.01 in., Step Height = 0.281 in., Ejection 10 degrees Down. P_0 = 313 psia, T_0 = 4,200°R, Re = 1.02×10^6

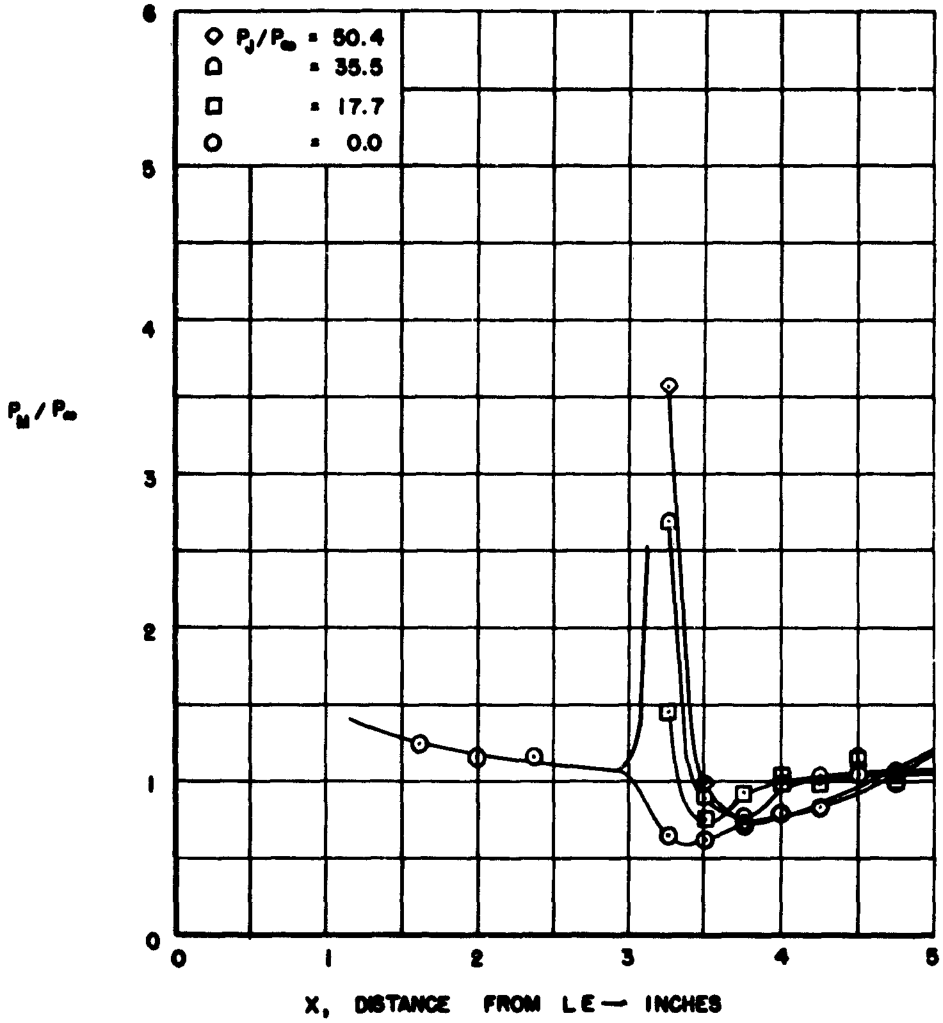

Figure 15a. **Pressure Distribution Over Model No. 6 at 0.0-degree Angle of Attack with Various Gas Ejection Pressures. L E Radius = 0.01 in., Step Height = 0.187 in. P_0 = 313 psia, T_0 = 3,300°R, Re = 1.42 x 10^6**

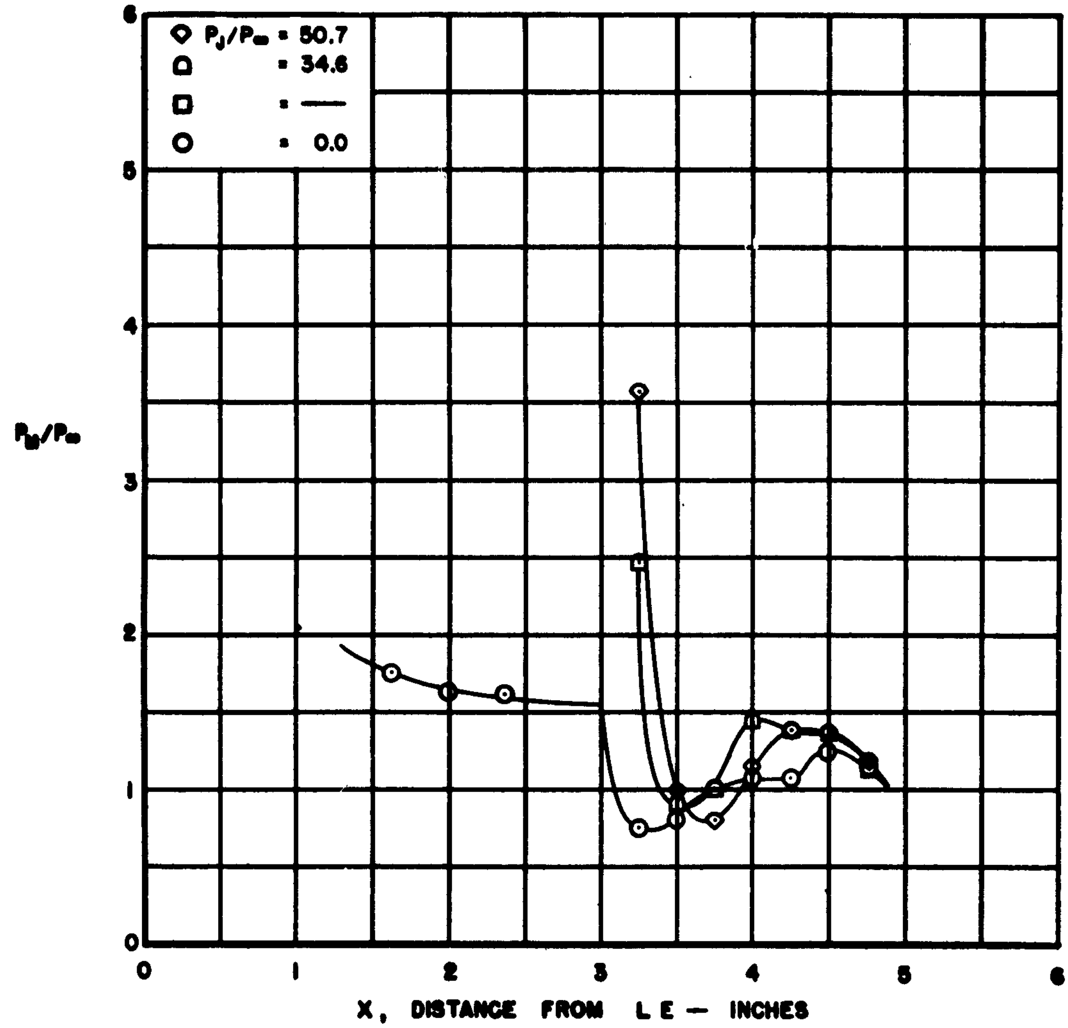

Figure 15b. Pressure Distribution Over Model No. 6 at -5.0-degree Angle of Attack with Various Gas Ejection Pressures. L E Radius = 0.01 in., Step Height = 0.187 in., P_0 = 313 psia, T_0 = 3,300°R, Re = 1.42×10^6

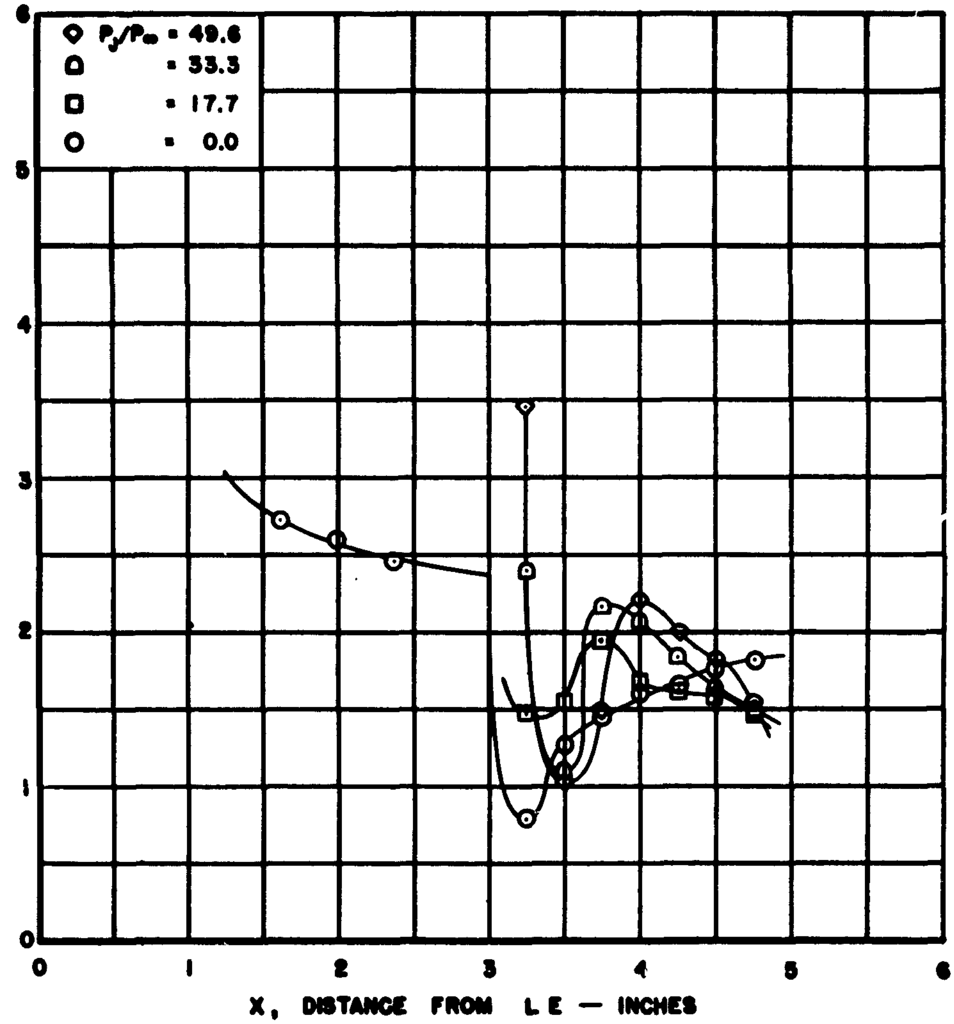

Figure 15c. Pressure Distribution Over Model No. 6 at -9.4-degree Angle of Attack with Various Gas Ejection Pressures. L E Radius = 0.01 in., Step Height = 0.187 in., P_0 = 313 psia, T_0 = 3,300°R, Re = 1.42 x 10^6

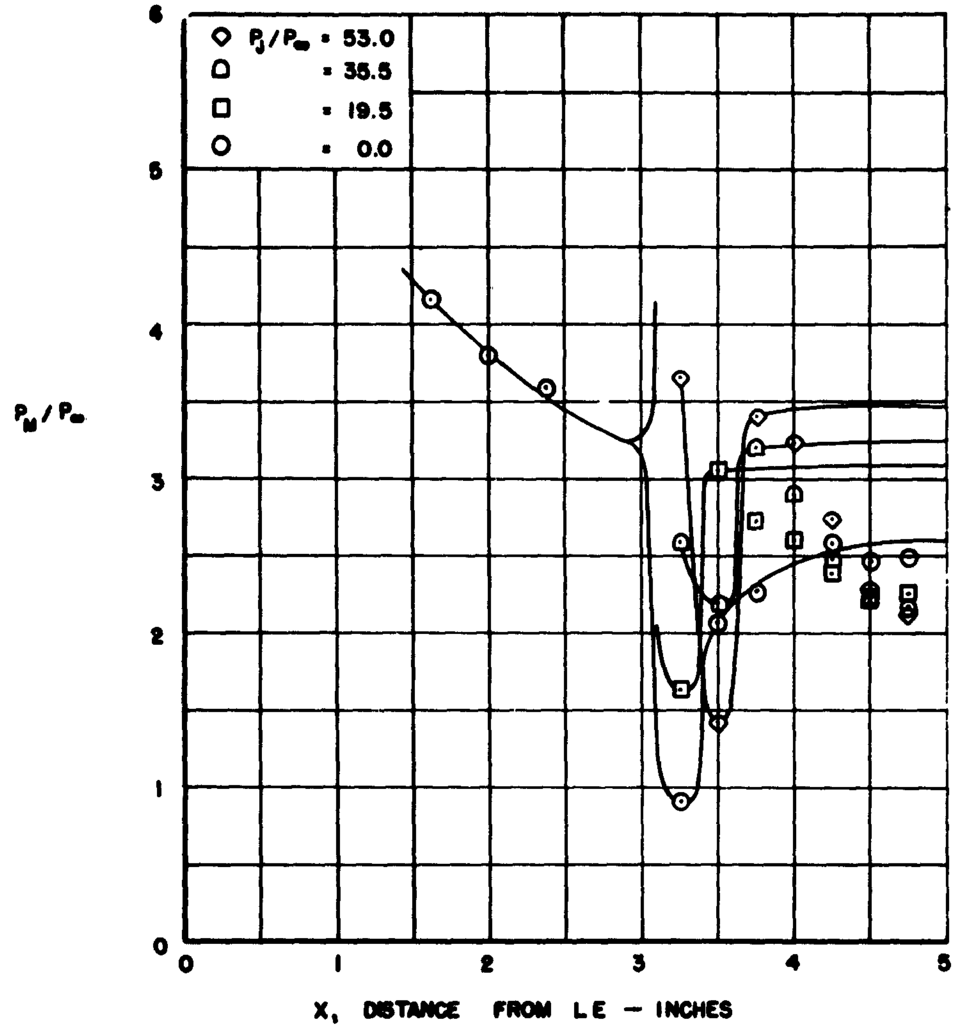

Figure 15d. Pressure Distribution Over Model No. 6 at -13.6-degree Angle of Attack with Various Gas Ejection Pressures. L E Radius = 0.01 in., Step Height = 0.187 in., P_0 = 313 psia, T_0 = 3,300°R, Re = 1.42×10^6

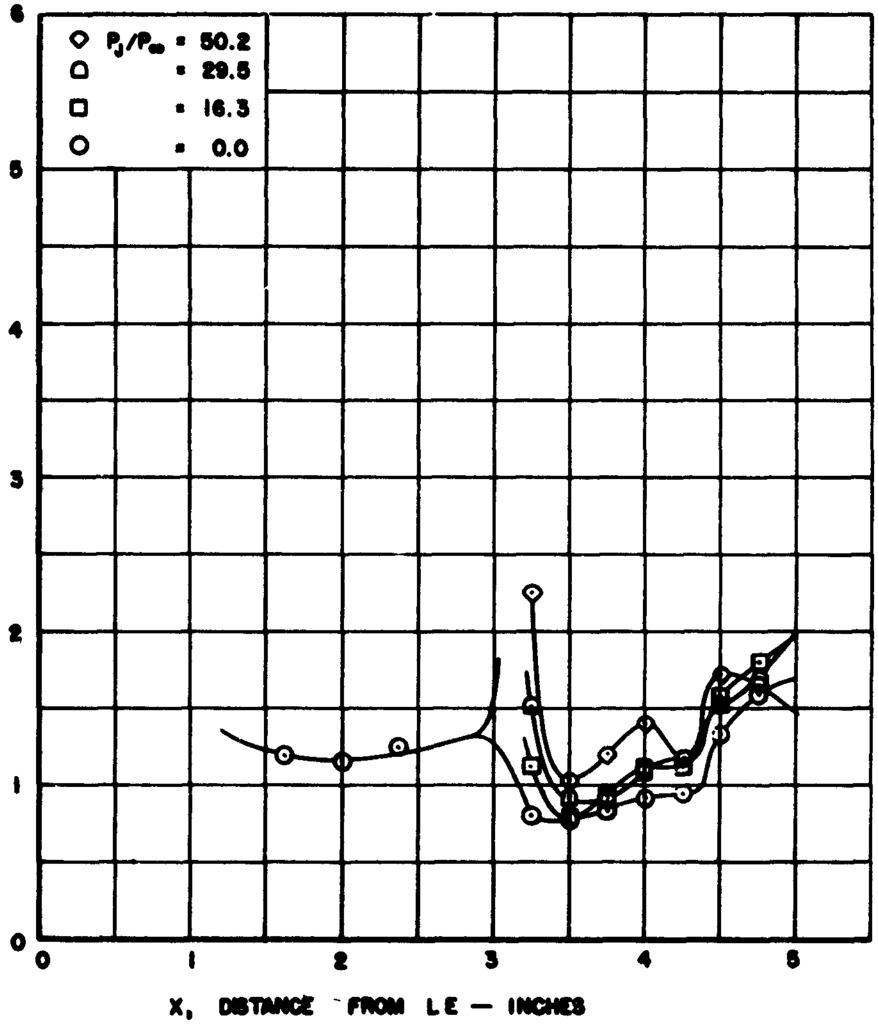

Figure 16a. Pressure Distribution Over Model No. 7 at 0.0-degree Angle of Attack with Various Gas Ejection Pressures. L E Radius = 0.01 in., Step Height = 0.187 in. Gas Ejection 10 degrees Up. P_0 = 312 psia, T_0 = 4,100°R, Re = 1.10 x 10^6

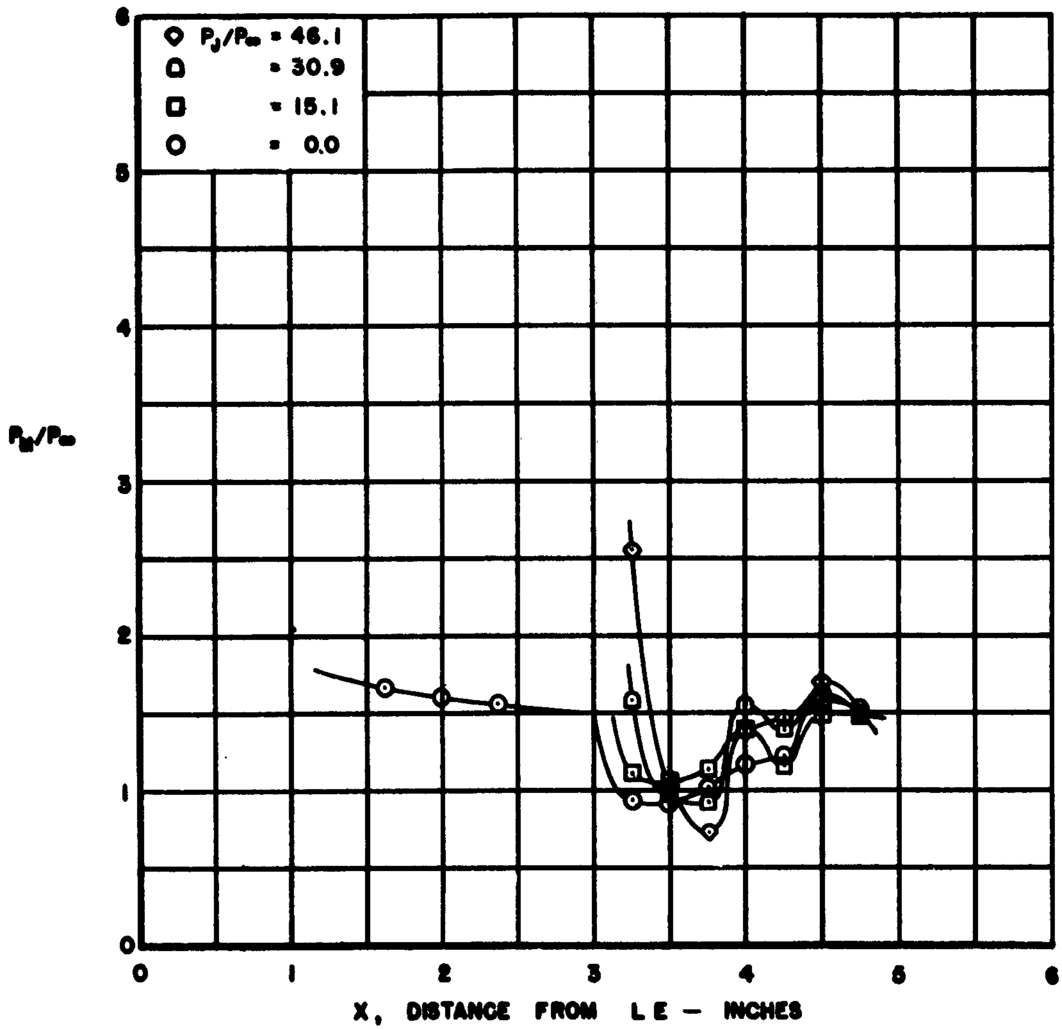

Figure 16b. Pressure Distribution Over Model No. 7 at -4.9-degree Angle of Attack with Various Gas Ejection Pressures. L E Radius = 0.01 in., Step Height = 0.187 in. Gas Ejection 10 degrees Up. P_0 = 312 psia, T_0 = 4,100°R, Re = 1.10×10^6

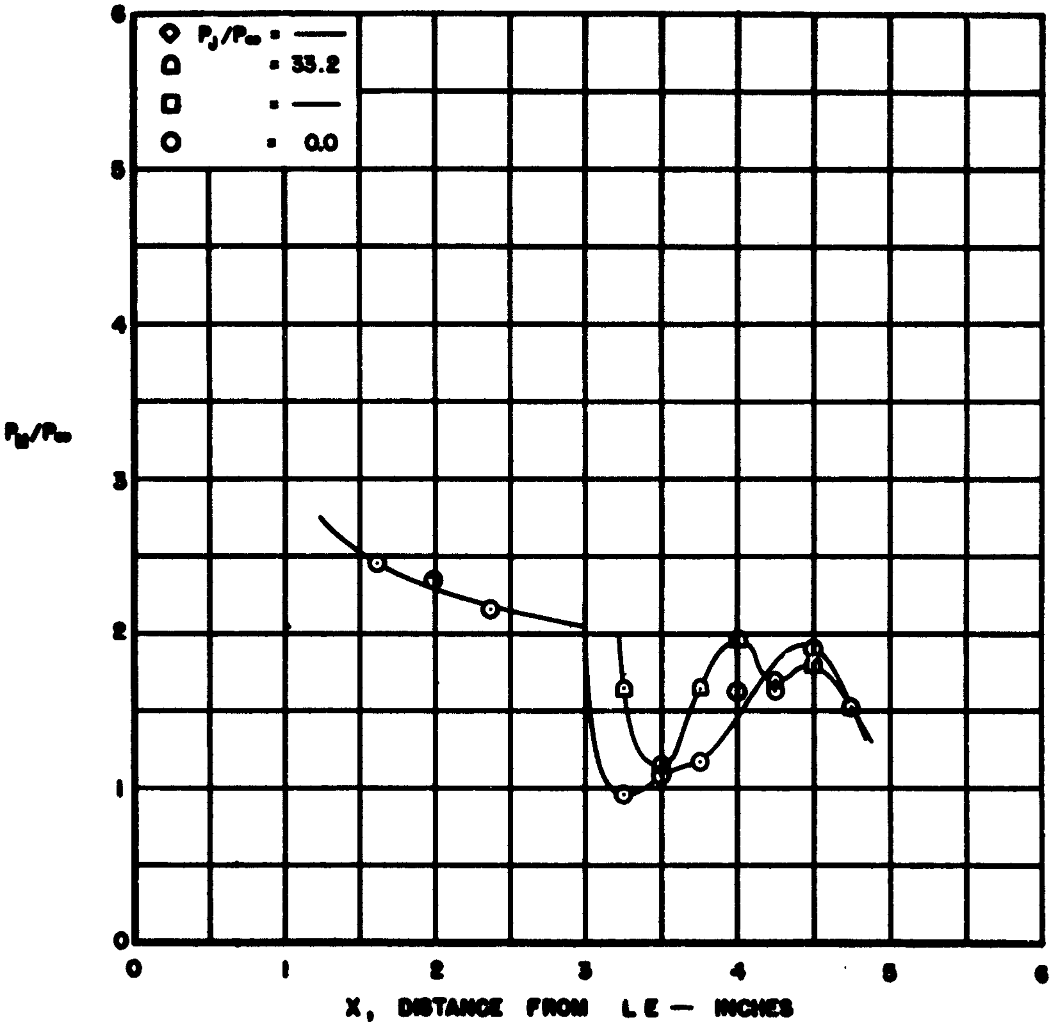

Figure 16c. Pressure Distribution Over Model No. 7 at -9.4-degree Angle of Attack with Various Gas Ejection Pressures. L E Radius = 0.01 in., Step Height = 0.187 in. Gas Ejection 10 degrees Up. P_0 = 312 psia, T_0 = 4,100°R, Re = 1.10 x 10^6

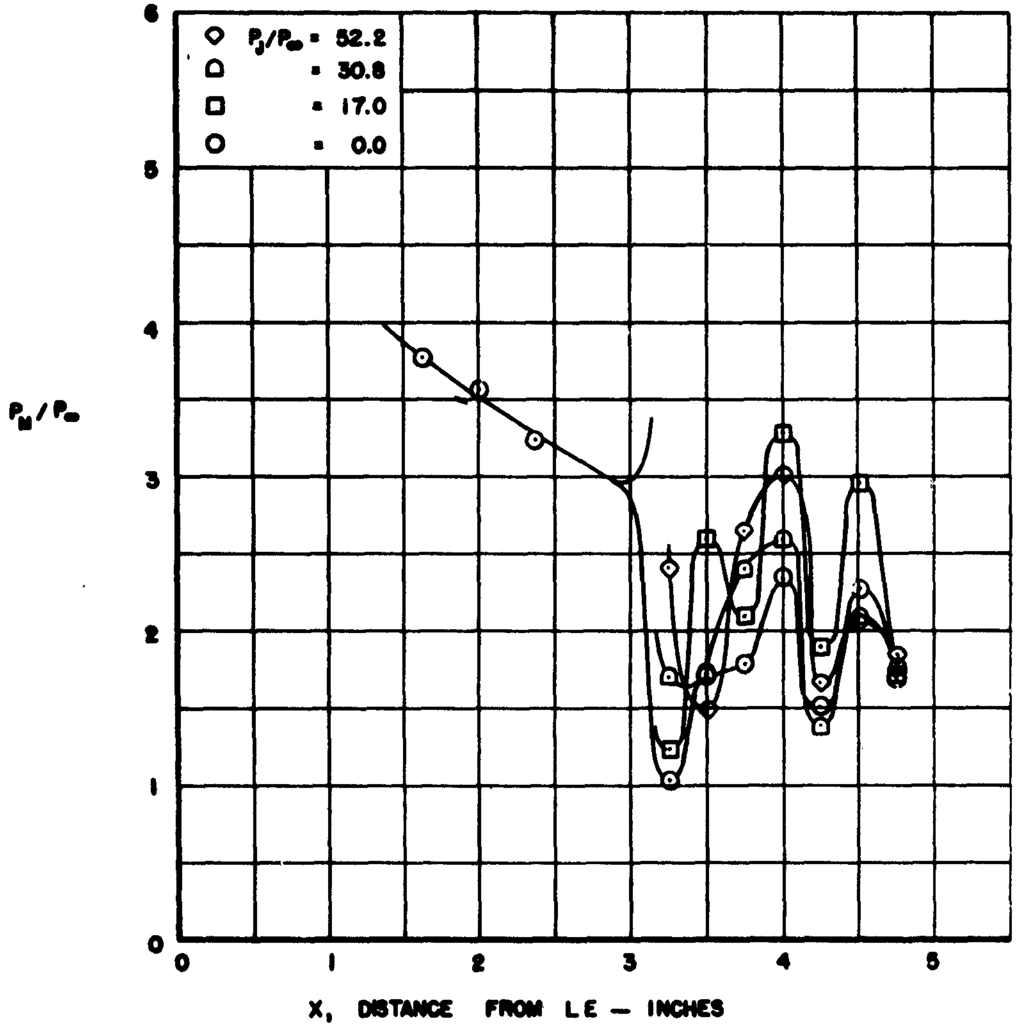

Figure 16d. Pressure Distribution Over Model No. 7 at -13.5-degree Angle of Attack with Various Gas Ejection Pressures. L E Radius = 0.01 in., Step Height = 0.187 in. Gas Ejection 10 degrees Up. P_0 = 312 psia, T_0 = 4,100°R, Re = 1.10×10^6

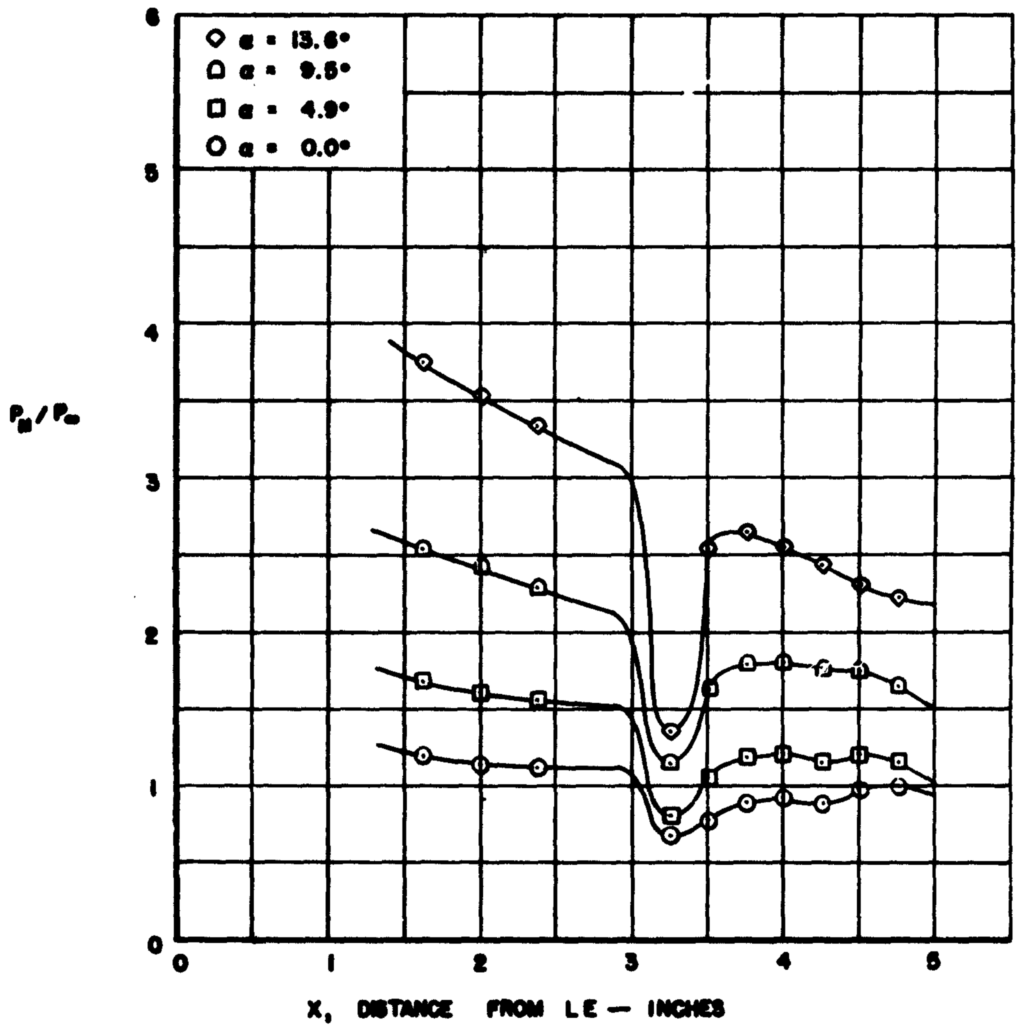

Figure 17. Pressure Distribution Over Model No. 8 at 0.0, -4.9, -9.5, and -13.6-degree Angles of Attack. L E Radius = 0.01 in., Step Height = 0.093 in. No Gas Ejection. P_0 = 314 psia, T_0 = 4,300°R, Re = 0.97 x 10^6

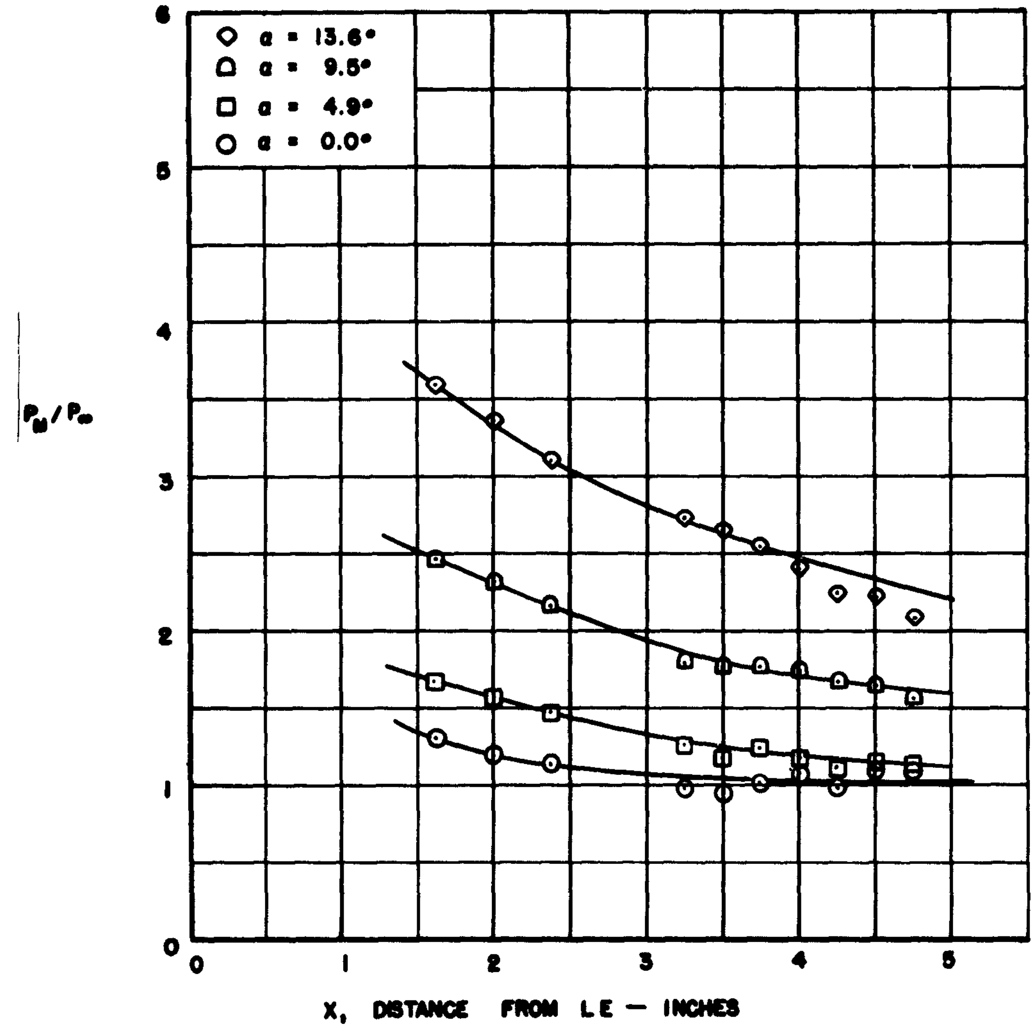

Figure 18. Pressure Distribution Over Model No. 9 at 0.0, -4.9, -9.5, and -13.6-degree Angles of Attack. L E Radius = 0.01, No Step. P_0 = 314 psia, T_0 = 4,300°R, Re = 0.97 x 10^6

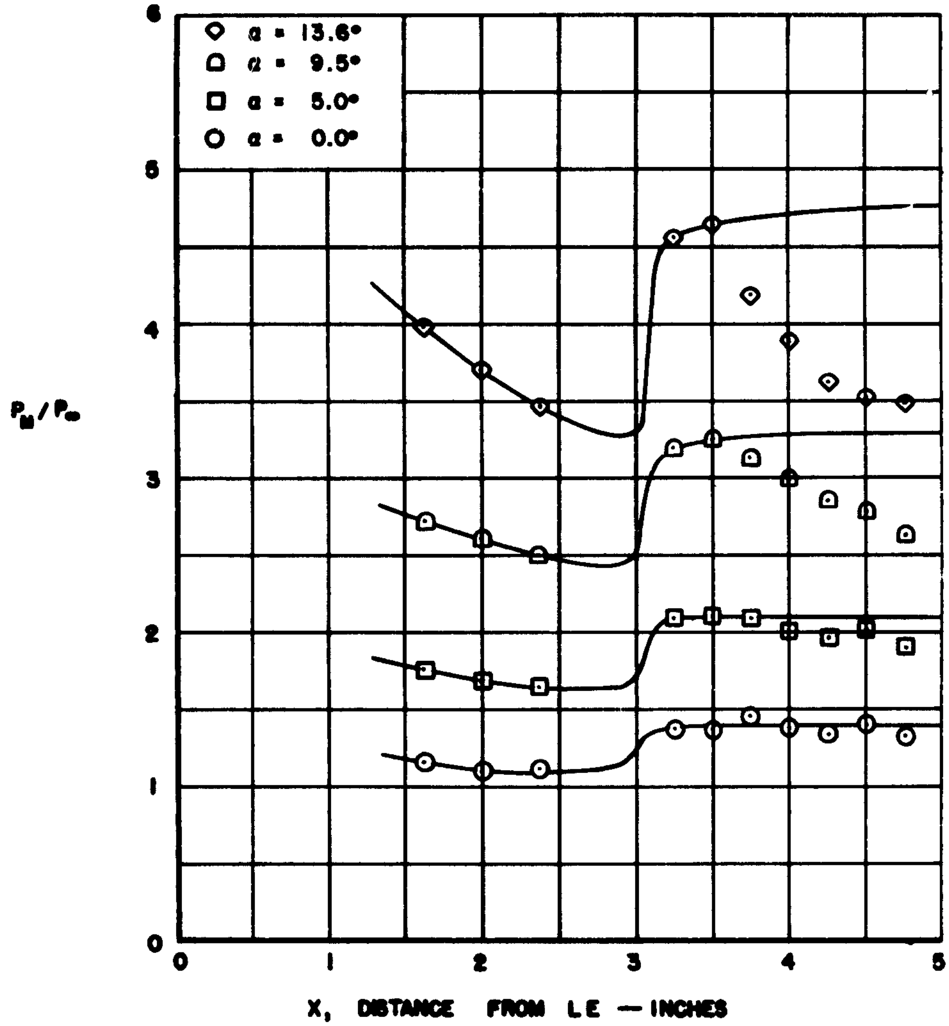

Figure 19. Pressure Distribution Over Model No. 10 at 0.0, -5.0, -9.5, and -13.6-degree Angles of Attack. L E Radius = 0.01 in., Ramp Angle = 5 degrees. P_0 = 312 psia, T_0 = 4,100°R, Re = 1.09 x 10^6

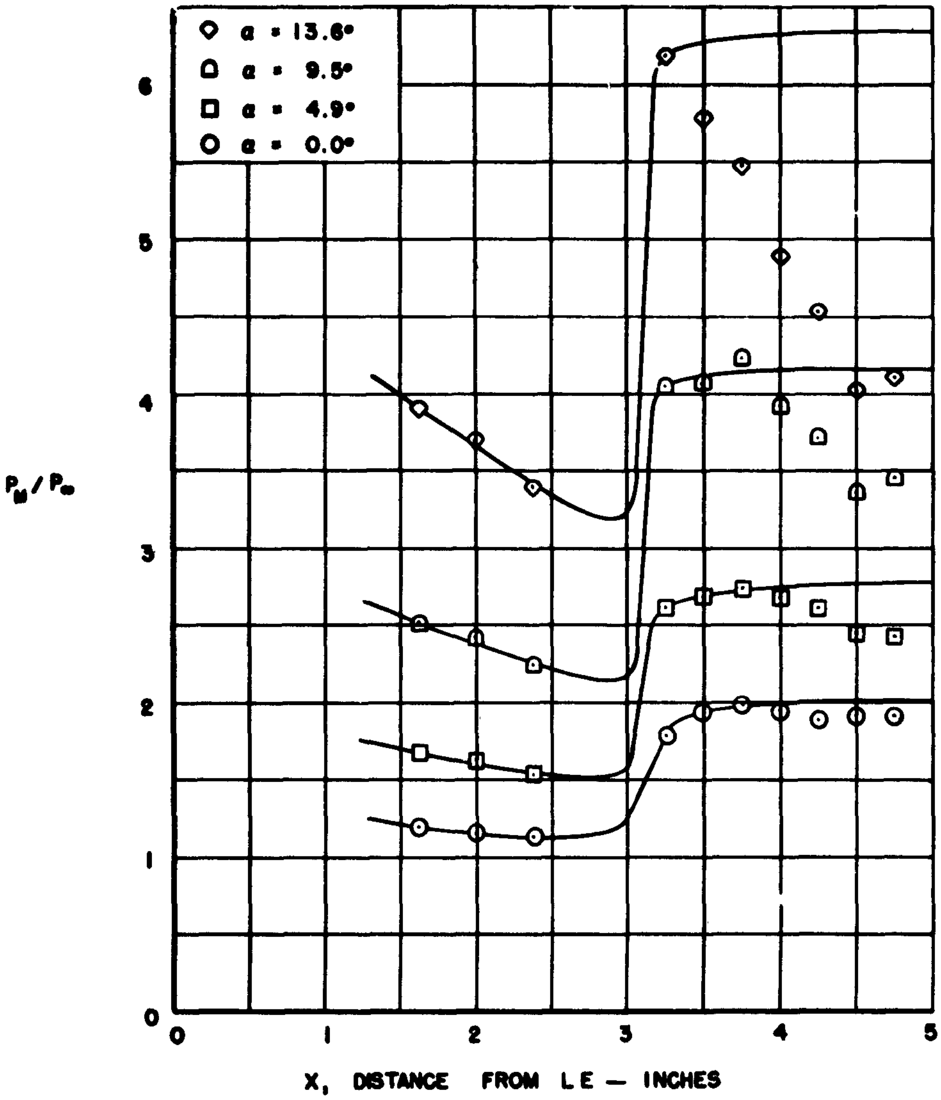

Figure 20. Pressure Distribution Over Model No. 11 at 0.0, -4.9, -9.5, and -13.6-degree Angles of Attack. L E Radius = 0.01 in., Ramp Angle = 10 degrees. P_0 = 314 psia, T_0 = 4,300°R, Re = 0.97 x 10^6

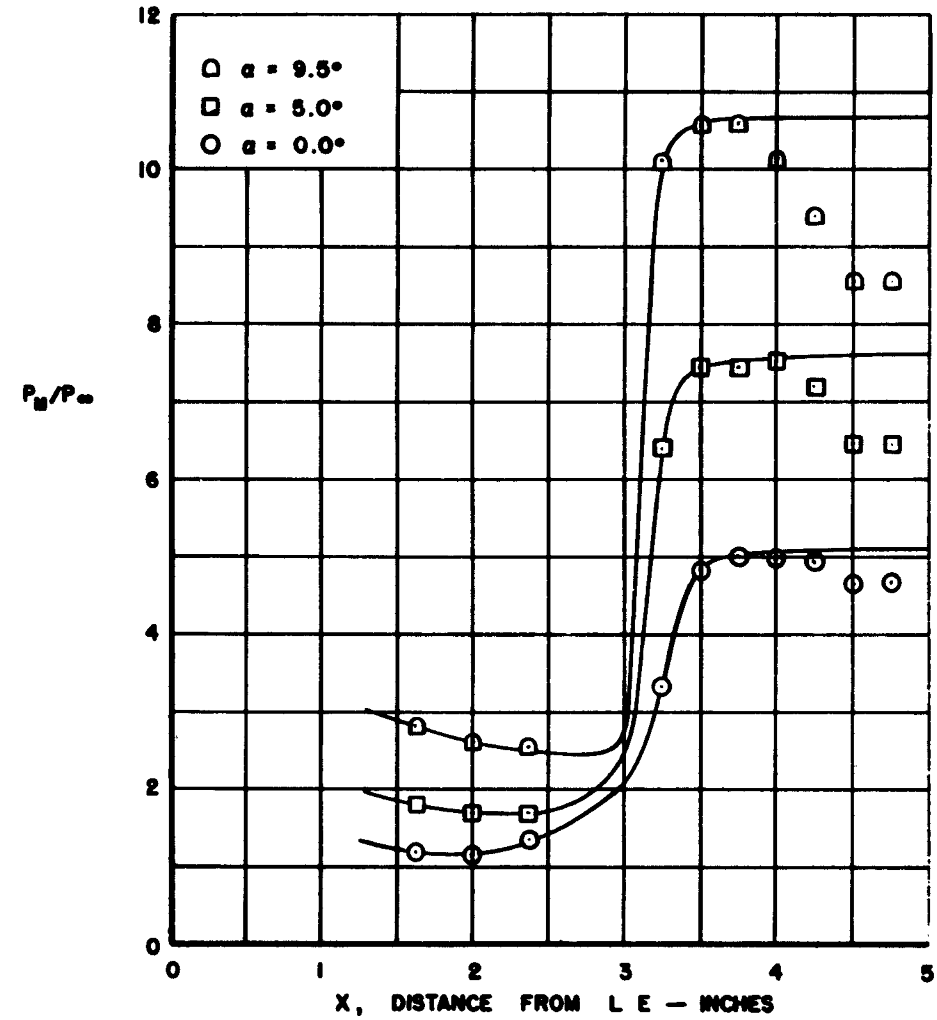

Figure 21. Pressure Distribution Over Model No. 12 at 0.0, -5.0, and -9.5-degree Angles of Attack. L E Radius = 0.01 in., Ramp Angle = 20 degrees. P_0 = 313 psia, T_0 = 3,300°R, Re = 1.42 x 10^6

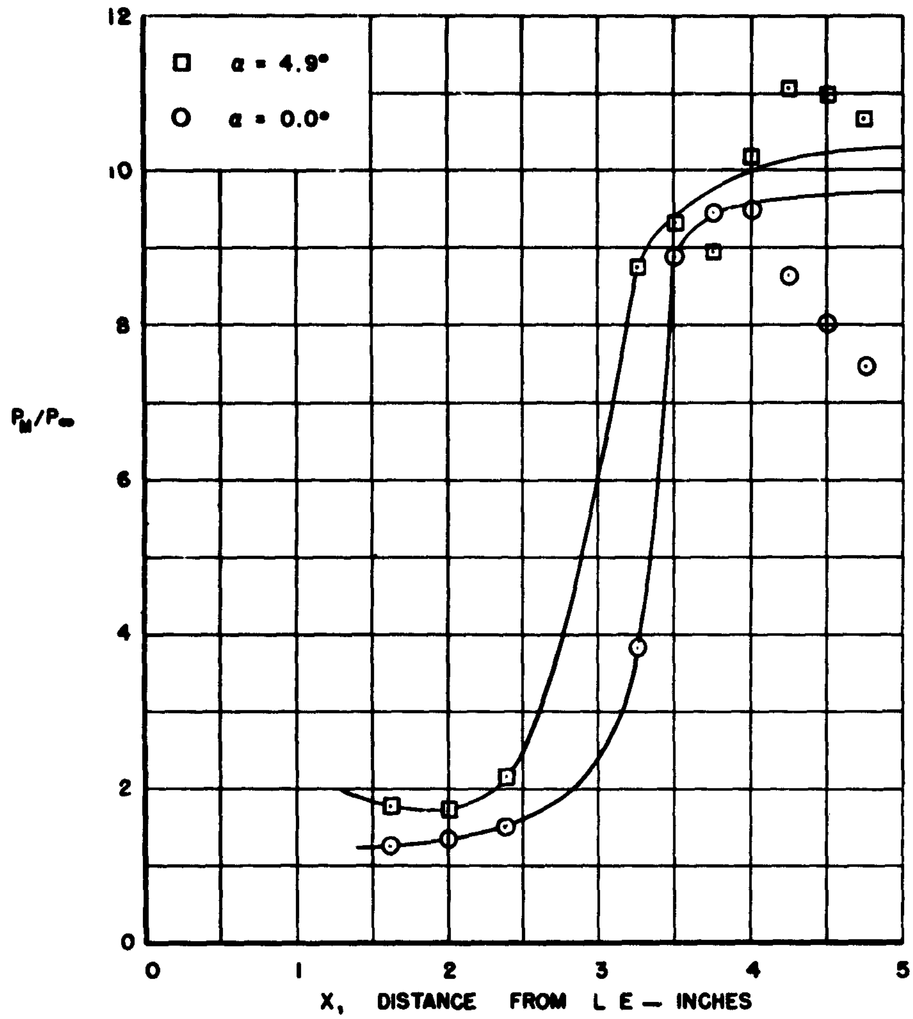

Figure 22. Pressure Distribution Over Model No. 13 at 0.0, and -4.9-degree Angles of Attack. L E Radius = 0.01 in., Ramp Angle = 30 degrees. P_0 = 312 psia, T_0 = 4,100°R, Re = 1.10 x 10^6

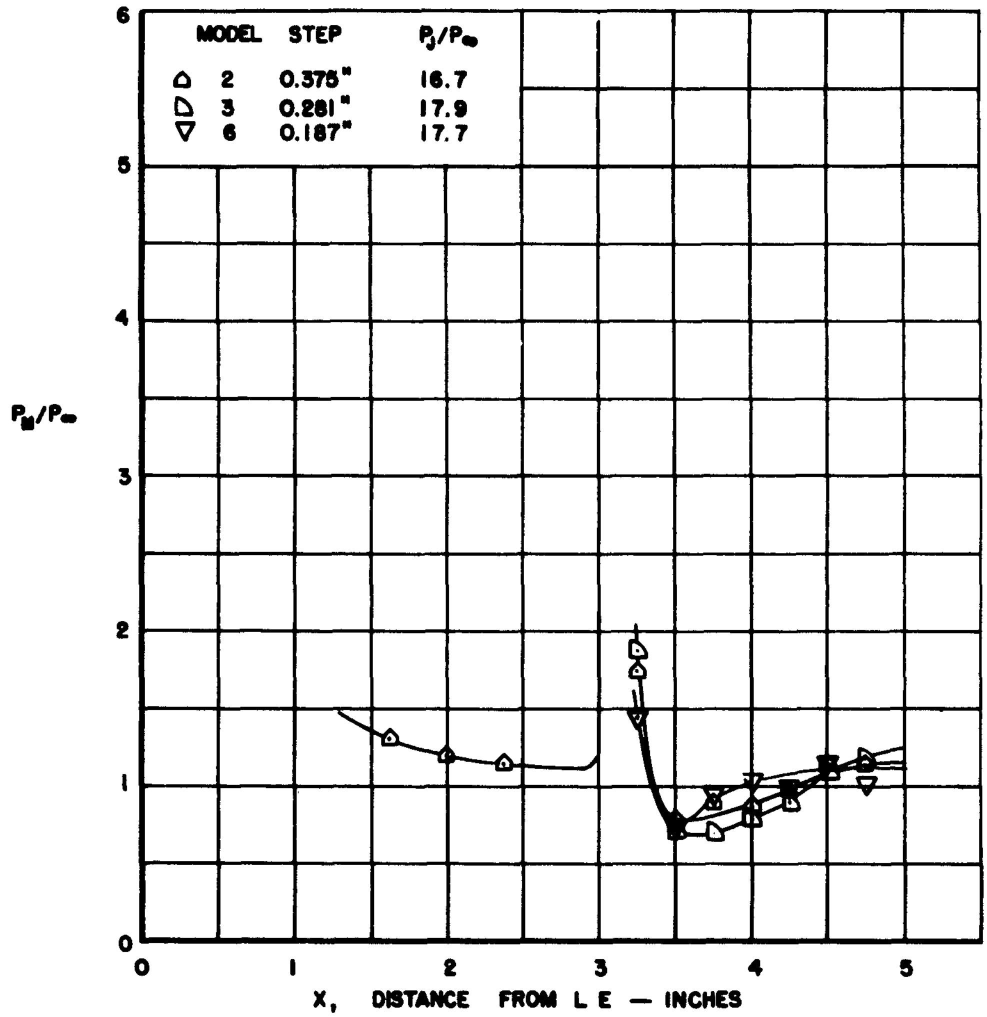

Figure 23. Effect of Step Height on Pressure Distribution Over 0.01 in. L E Radius Models at 0.0-degree Angle of Attack. $P_j/P_\infty \sim 17$

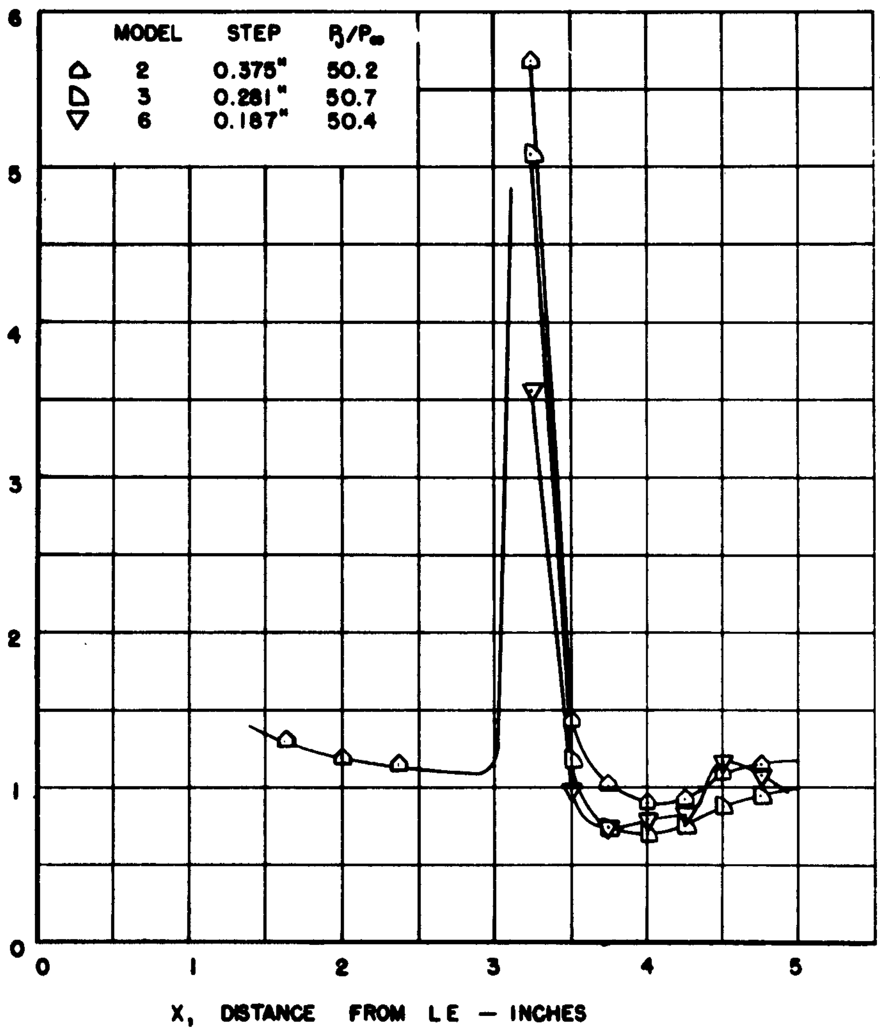

Figure 24. Effect of Step Height on Pressure Distribution Over 0.01 in. L E Radius Models at 0.0-degree Angle of Attack. $P_j/P_\infty \sim 50$

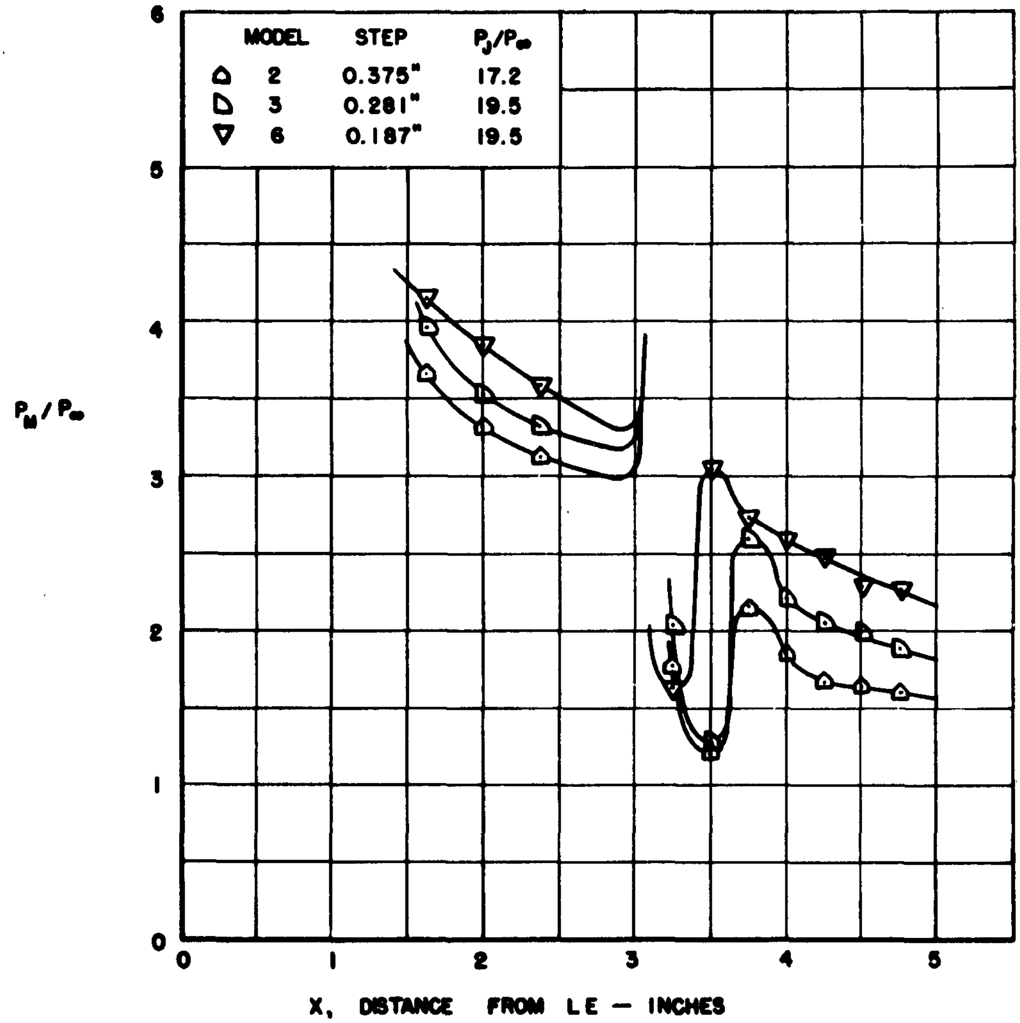

Figure 25. Effect of Step Height on Pressure Distribution Over 0.01 in. L E Radius Models at -13.6-degree Angle of Attack. $P_j/P_\infty \sim 19$

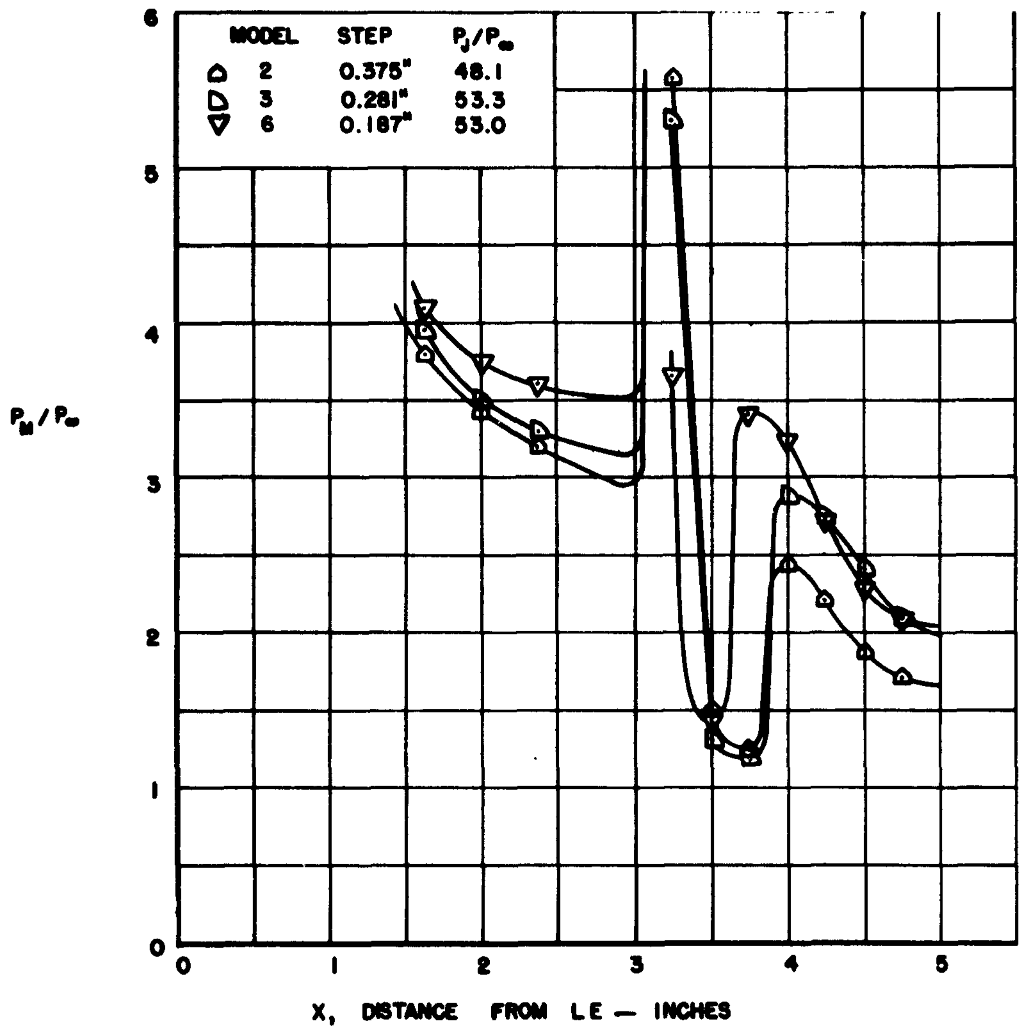

Figure 26. Effect of Step Height on Pressure Distribution Over 0.01 in. L E Radius Models at -13.6-degree Angle of Attack. $P_j/P_\infty \sim 53$

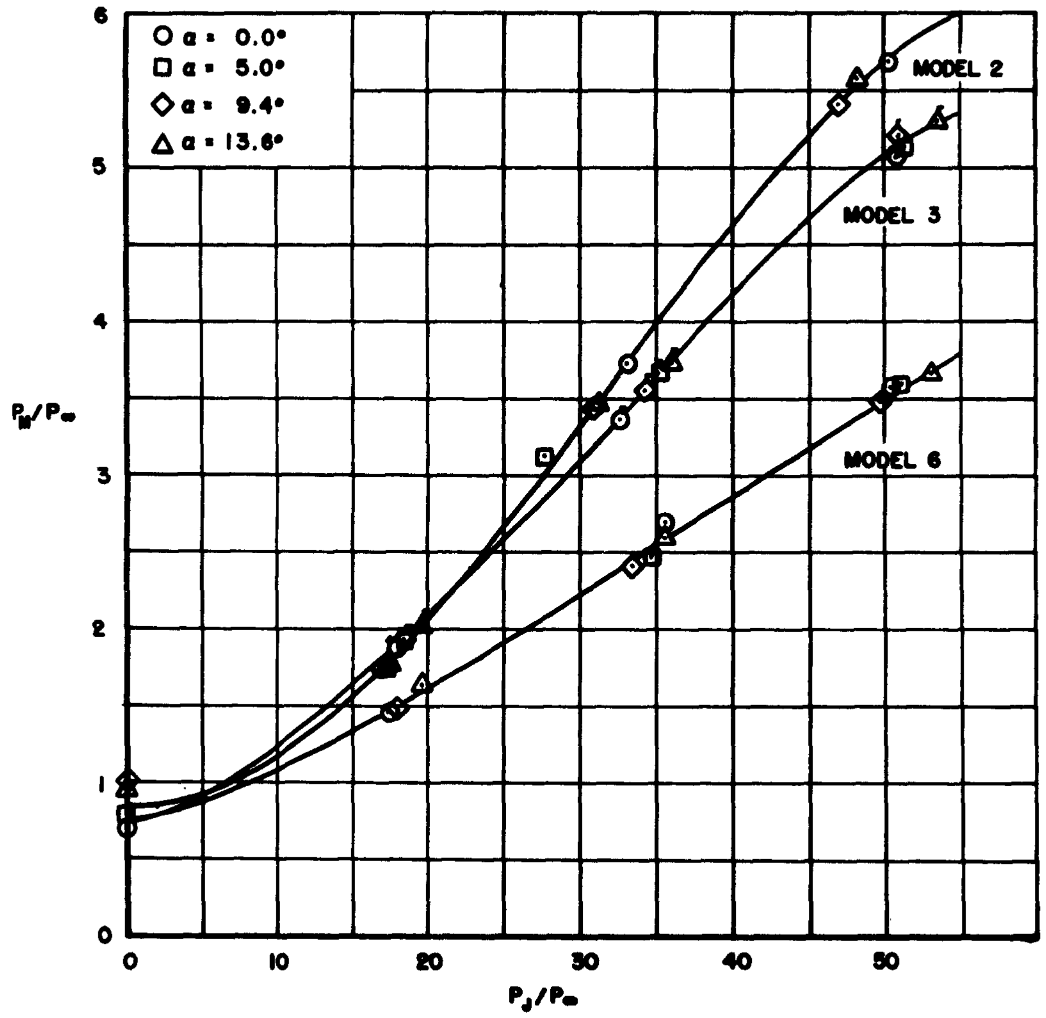

Figure 27. Effect of Step Height on Pressure at Orifice No. 5 (X = 3.25 in.), Immediately Behind Step, Model No. 2 - 0.375 in. Step, Model No. 3 - 0.281 in. Step. Model No. 6 - 0.187 in. Step.

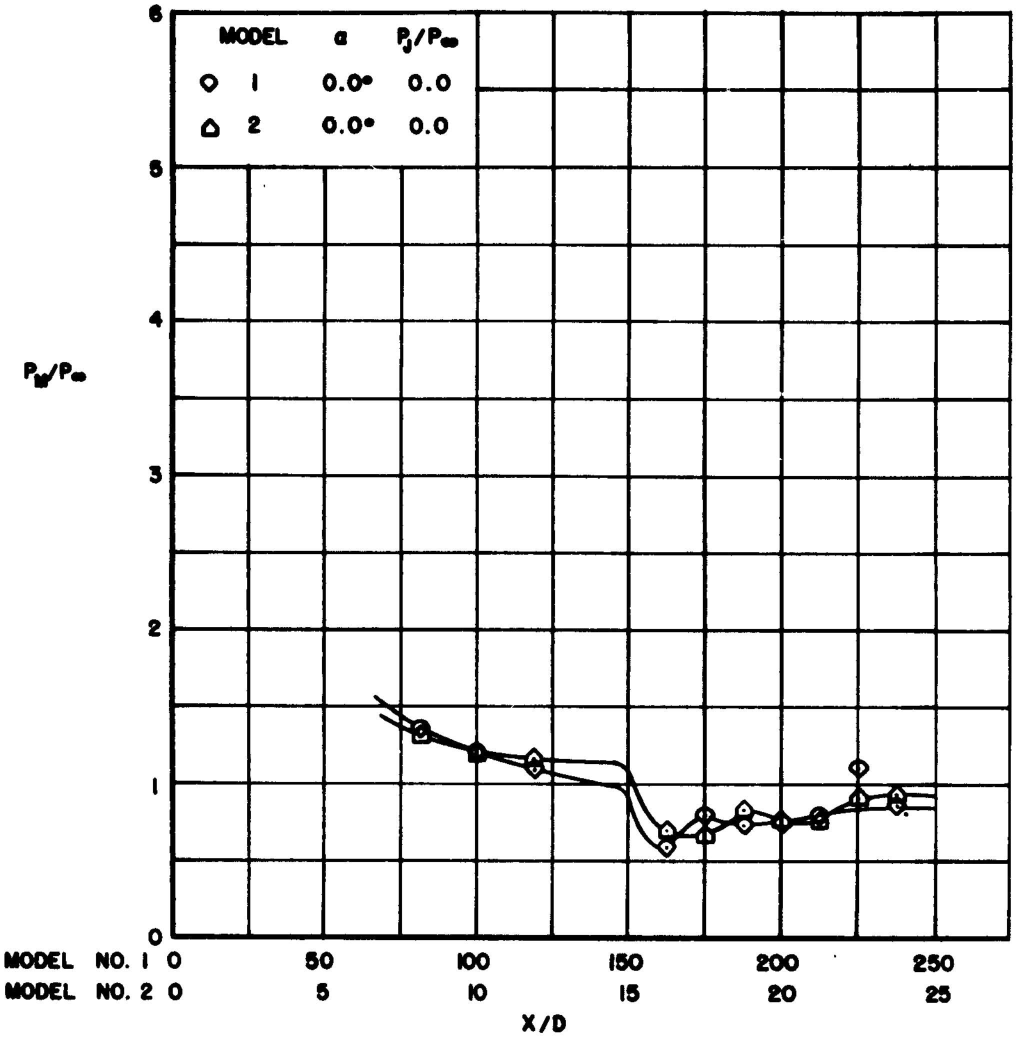

Figure 28. Effect of L E Blunting on Pressure Distribution Over 0.375 in. Step Models at 0.0-degree Angle of Attack. $P_j/P_\infty \sim 0$. P_0 = 311 psia, T_0 = 4,100°R, Re = 1.09×10^6

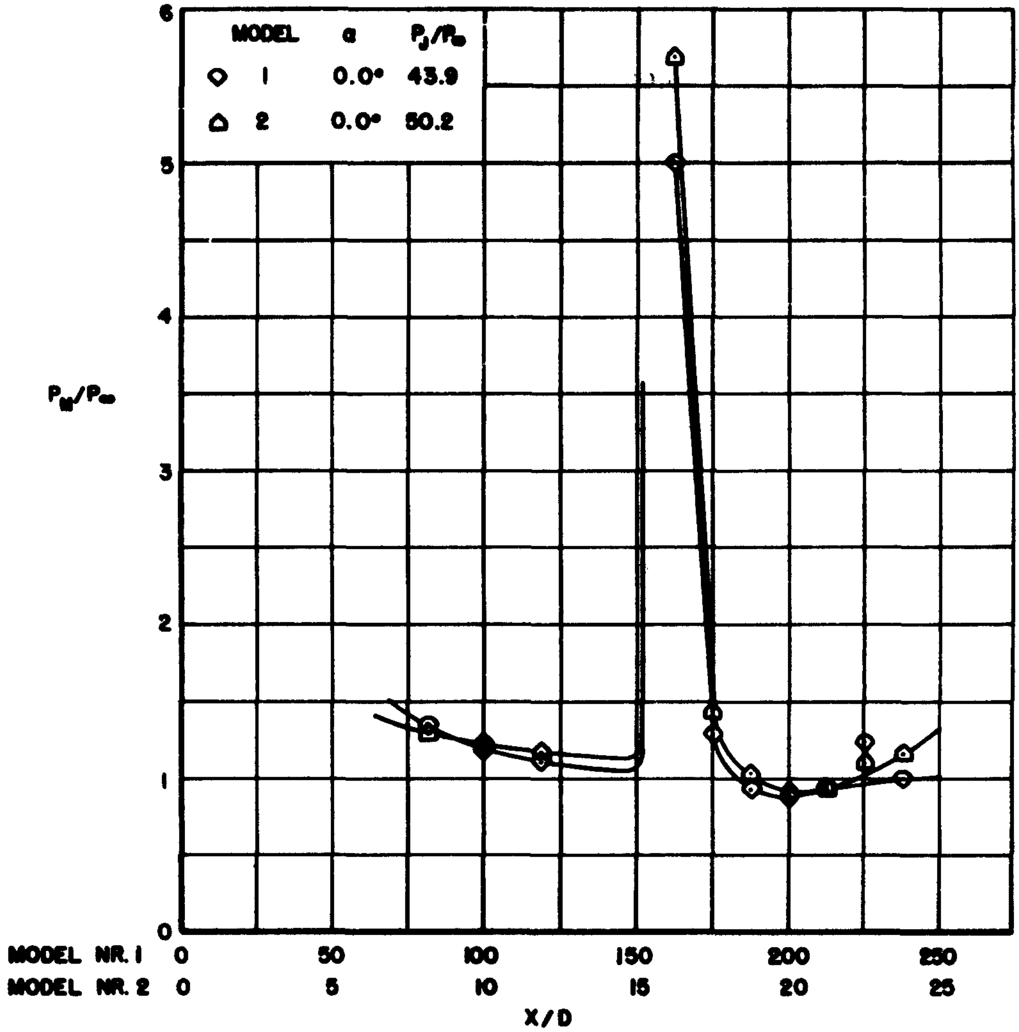

Figure 29. Effect of L E Blunting on Pressure Distribution Over 0.375 in. Step Models at 0.0-degree Angle of Attack. $P_j/P_\infty \sim 45$. $P_0 = 311$ psia, $T_0 = 4,100°R$, $Re = 1.09 \times 10^6$

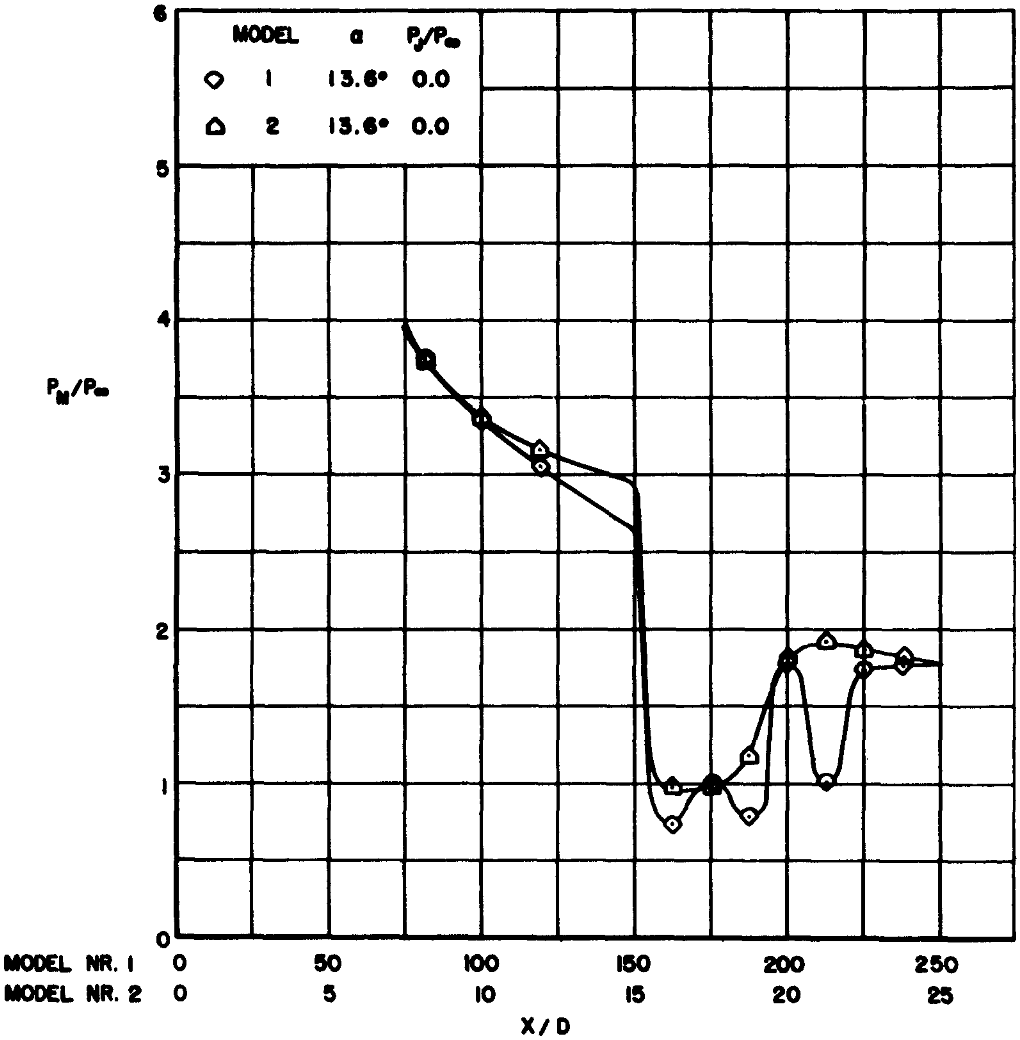

Figure 30. Effect of L E Blunting on Pressure Distribution Over 0.375 in. Step Models at -13.6-degree Angle of Attack. $P_j/P_\infty \sim 0$. P_0 = 311 psia, T_0 = 4,100°R, Re = 1.09×10^6

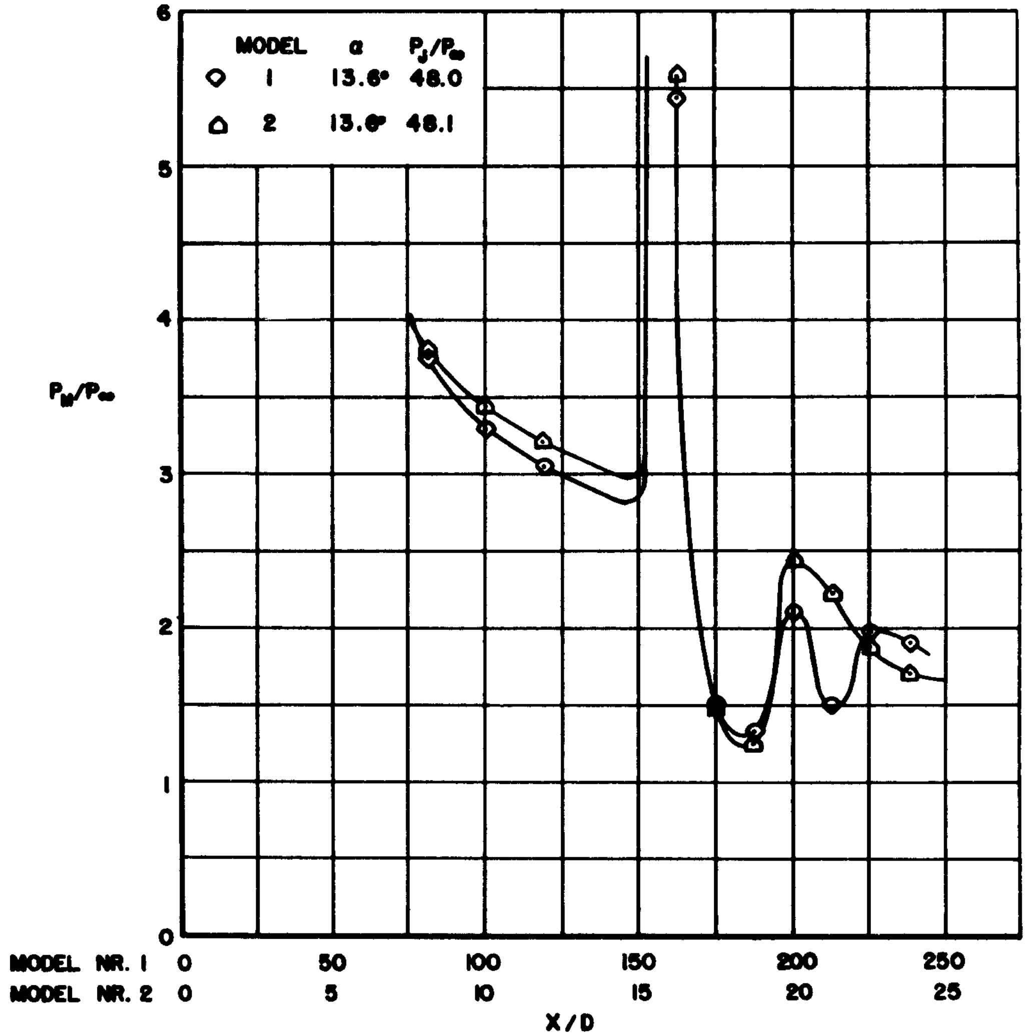

Figure 31. Effect of L E Blunting on Pressure Distribution Over 0.375 in. Step Models at -13.6-degree Angle of Attack. $P_j/P_\infty \sim 48$. P_0 = 311 psia, T_0 = 4,100°R, Re = 1.09×10^6

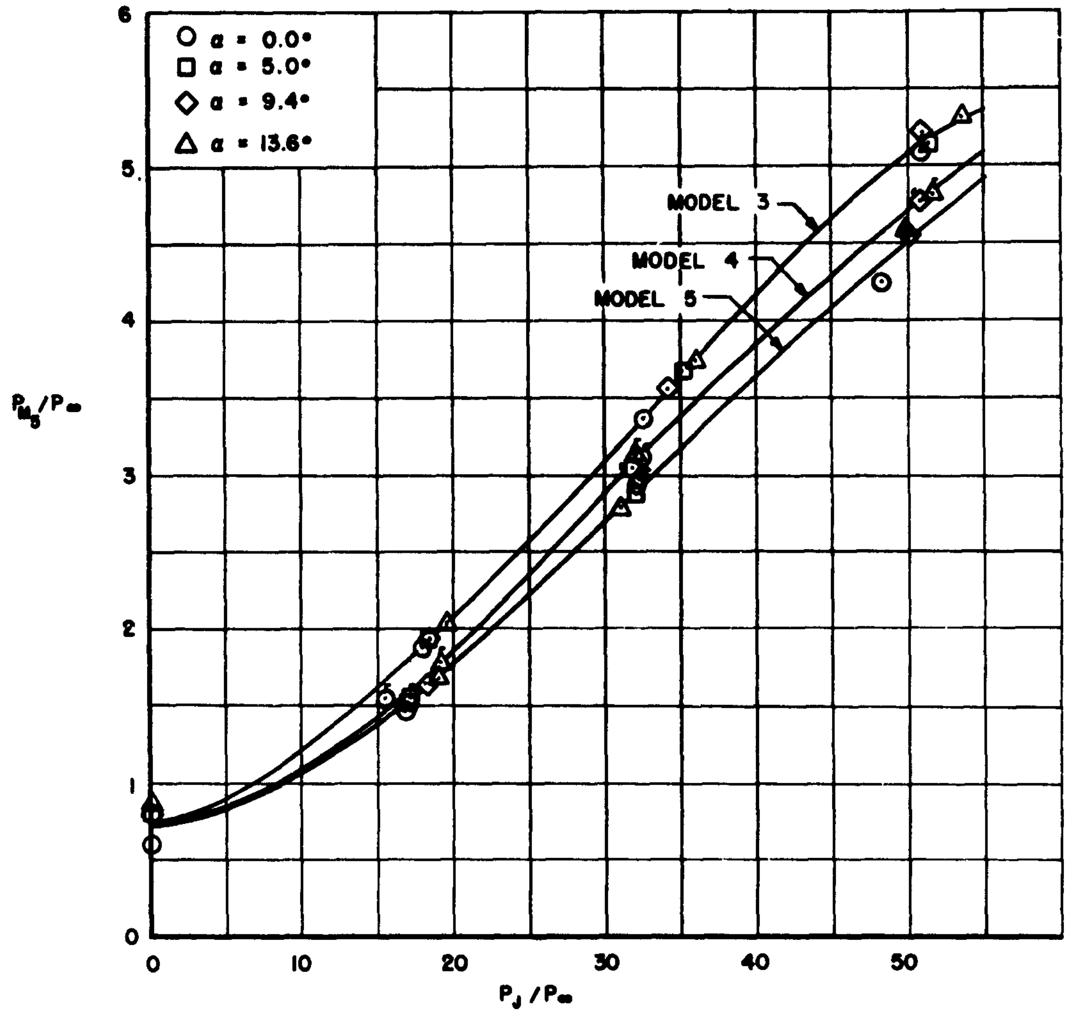

Figure 32. Effect of Gas Ejection Angle on the Pressure at Orifice No. 5 (X = 3.25 in.), Immediately Behind the Step. 0.281 in. Step Height. Model No. 3 - Ejection Parallel to Surface, Model No. 4 - Ejection 10 degrees Up, Model No. 5 - Ejection 10 degrees Down.

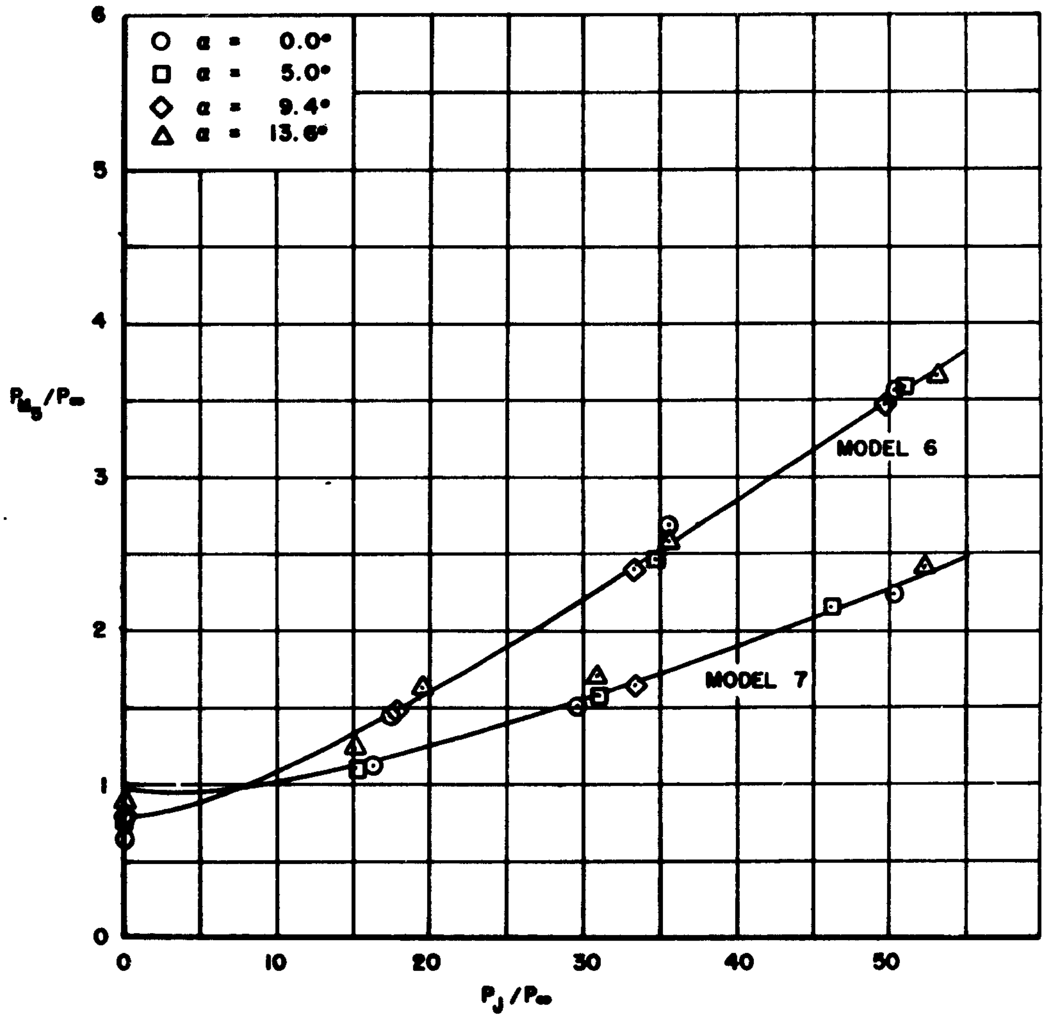

Figure 33. Effect of Gas Ejection Angle on the Pressure at Orifice No. 5 (X = 3.25 in.), Immediately Behind the Step. 0.187 in. Step Height Model No. 6 - Ejection Parallel to Surface, Model No. 7 - Ejection 10 degrees Up.

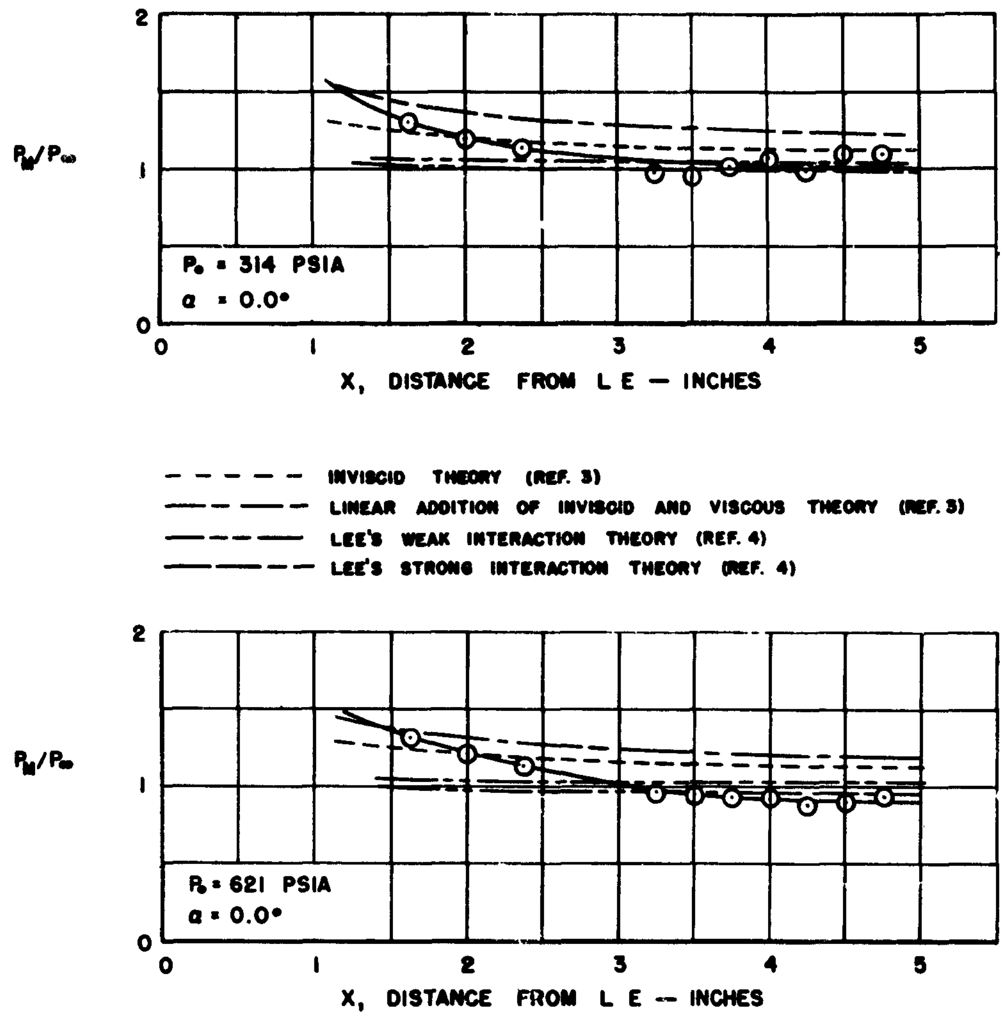

Figure 34. Comparison of HTF Flat Plate Results with Theory

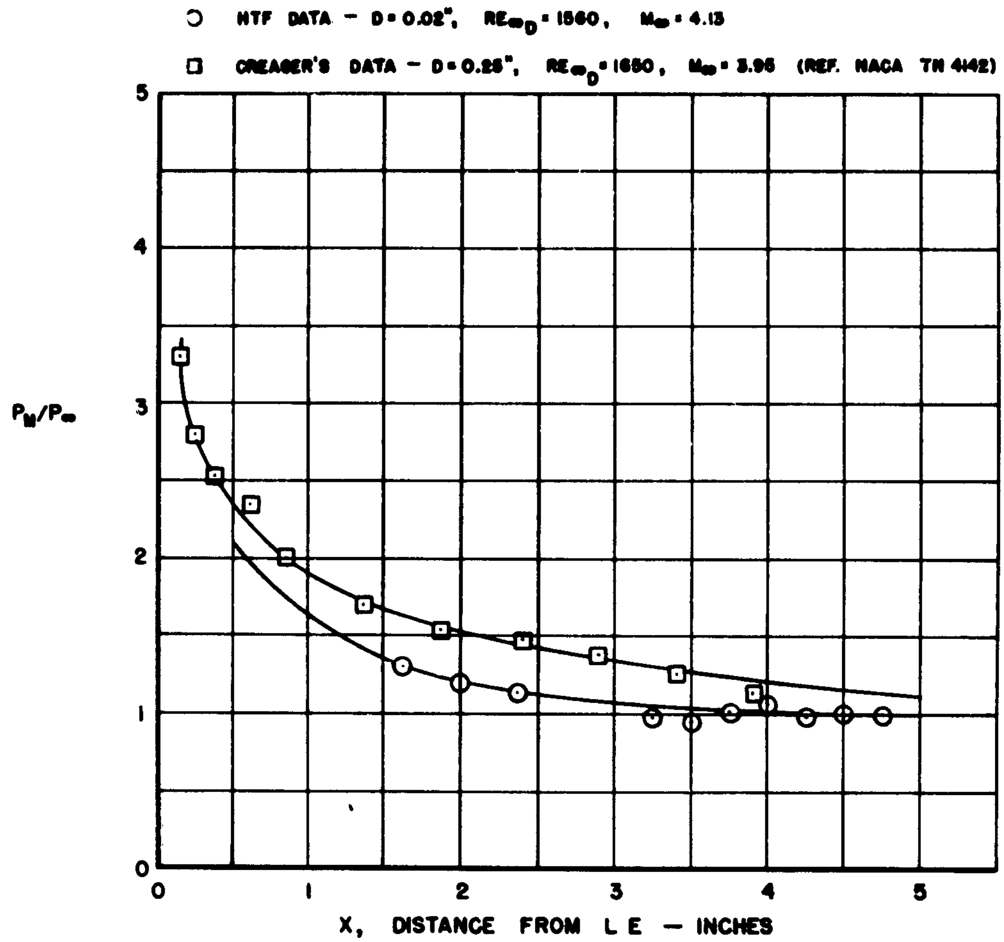

Figure 35. Comparison of HTF Flat Plate Results with Experimental Data

Aeronautical Systems Division, Directorate of Engineering Test, Deputy for Test and Support, Wright-Patterson AFB, Ohio.
Rpt Nr ASD-TDR-63-131, INVESTIGATION OF FLOW VARIABLES OVER A SERIES OF REARWARD FACING STEPPED FLAT PLATES AT A NOMINAL MACH NUMBER OF 4.15. Final report, Apr. 63, 72p. incl illus., tables, 8 refs.

Unclassified Report

A study was made of the aerodynamic characteristics over a flat plate with basic changes in the flow field imposed by geometric and aerodynamic means. Pressure distributions and schlieren photographs were used to show the

(over)

effects of (1) leading edge bluntness, (2) rearward facing step, (3) rearward facing step with gas ejected from the vertical face of the step, and (4) a control surface. Although three dimensional effects were large at high angles of attack, the flat plate results correlated well with theory and other experimental data. The effects of leading edge bluntness, step height, and ejection angle are small. The effect of gas ejection, in the manner tested, is not sufficient to produce the effect of a physical control surface.

1. Hypersonic Flow
2. Fluid Mechanics (gas)
3. Aerodynamic Characteristics
4. Flat Plates With Gas Ejection

I. AFSC Project 1366, Task 136607
II. Richard R. Smith
III. Aval fr OTS
IV. In ASTIA collection

Aeronautical Systems Division, Directorate of Engineering Test, Deputy for Test and Support, Wright-Patterson AFB, Ohio.
Rpt Nr ASD-TDR-63-131, INVESTIGATION OF FLOW VARIABLES OVER A SERIES OF REARWARD FACING STEPPED FLAT PLATES AT A NOMINAL MACH NUMBER OF 4.15. Final report, Apr. 63, 72p. incl illus., tables, 8 refs.

Unclassified Report

A study was made of the aerodynamic characteristics over a flat plate with basic changes in the flow field imposed by geometric and aerodynamic means. Pressure distributions and schlieren photographs were used to show the

(over)

effects of (1) leading edge bluntness, (2) rearward facing step, (3) rearward facing step with gas ejected from the vertical face of the step, and (4) a control surface. Although three dimensional effects were large at high angles of attack, the flat plate results correlated well with theory and other experimental data. The effects of leading edge bluntness, step height, and ejection angle are small. The effect of gas ejection, in the manner tested, is not sufficient to produce the effect of a physical control surface.

1. Hypersonic Flow
2. Fluid Mechanics (gas)
3. Aerodynamic Characteristics
4. Flat Plates With Gas Ejection

I. AFSC Project 1366, Task 136607
II. Richard R. Smith
III. Aval fr OTS
IV. In ASTIA collection